

# Surveying the mass spectra and the electromagnetic properties of the $\Xi_c^{(*)}D^{(*)}$ molecular pentaquarks

Fu-Lai Wang<sup>1,2,3,5\*</sup> and Xiang Liu<sup>1,2,3,4,5†</sup>

<sup>1</sup>*School of Physical Science and Technology, Lanzhou University, Lanzhou 730000, China*

<sup>2</sup>*Lanzhou Center for Theoretical Physics, Key Laboratory of Theoretical Physics of Gansu Province, Lanzhou University, Lanzhou 730000, China*

<sup>3</sup>*Key Laboratory of Quantum Theory and Applications of MoE, Lanzhou University, Lanzhou 730000, China*

<sup>4</sup>*MoE Frontiers Science Center for Rare Isotopes, Lanzhou University, Lanzhou 730000, China*

<sup>5</sup>*Research Center for Hadron and CSR Physics, Lanzhou University and Institute of Modern Physics of CAS, Lanzhou 730000, China*

Inspired by the observed  $P_{\psi_s}^\Lambda(4459)/P_{\psi_s}^\Lambda(4338)$  and  $T_{cc}(3875)^+$  states as the  $\Xi_c\bar{D}^*/\Xi_c\bar{D}$  and  $DD^*$  molecular candidates, respectively, in this work we investigate the  $\Xi_c^{(*)}D^{(*)}$  molecular systems. We obtain the mass spectra and the corresponding spatial wave functions of the  $\Xi_c^{(*)}D^{(*)}$ -type double-charm molecular pentaquark candidates with single strangeness, where we employ the one-boson-exchange model and take into account both the  $S$ - $D$  wave mixing effect and the coupled channel effect. Our results suggest that the most promising candidates of the double-charm molecular pentaquarks with single strangeness include the  $\Xi_c D$  state with  $I(J^P) = 0(1/2^-)$ , the  $\Xi'_c D$  state with  $I(J^P) = 0(1/2^-)$ , the  $\Xi_c D^*$  states with  $I(J^P) = 0(1/2^-, 3/2^-)$ , the  $\Xi'_c D^*$  state with  $I(J^P) = 0(3/2^-)$ , the  $\Xi_c D^*$  states with  $I(J^P) = 0(1/2^-, 3/2^-)$ , and the  $\Xi'_c D^*$  states with  $I(J^P) = 0(1/2^-, 3/2^-, 5/2^-)$ . To gain further insight into the inner structures and the properties of the isoscalar  $\Xi_c^{(*)}D^{(*)}$  molecular candidates, we utilize the constituent quark model to analyze their M1 radiative decay behaviors and magnetic moments based on the obtained mass spectra and spatial wave functions, which can offer the significant information to determine their spin-parity quantum numbers and configurations in the forthcoming experiments. We suggest our experimental colleagues to search for the predicted  $\Xi_c^{(*)}D^{(*)}$  molecular states.

## I. INTRODUCTION

The search for exotic hadronic matter is a challenging and rewarding research topic of hadron spectroscopy. The first observation of the charmonium-like XYZ state, the  $X(3872)$ , was reported by the Belle Collaboration in 2003 [1]. In the last two decades, a number of new hadronic states have been observed in different experiments as summarized in reviews [2–12]. We may notice an interesting phenomenon, where some observed new hadronic states are close to the threshold of two hadrons. It is natural to propose that these new hadronic states can be as good candidates for hadronic molecular states [2–12], which are beyond the conventional hadrons [13, 14]. A typical example is the discovery of three hidden-charm pentaquark states, named as the  $P_{\psi}^N(4312)$ ,  $P_{\psi}^N(4440)$ , and  $P_{\psi}^N(4457)$ , which exist in the  $J/\psi p$  invariant mass spectrum of the  $\Lambda_b^0 \rightarrow J/\psi p K^-$  decay [15]. It provides a direct support for the existence of molecular-type hidden-charm pentaquark states, which are relevant to the  $\Sigma_c \bar{D}^{(*)}$  interaction [16–22].

Subsequently, two hidden-charm pentaquark states with strangeness, the  $P_{\psi_s}^\Lambda(4459)$  [23] and  $P_{\psi_s}^\Lambda(4338)$  [24], were announced by the LHCb Collaboration. This is a good opportunity to briefly present the research status of them. In 2021, the  $P_{\psi_s}^\Lambda(4459)$  [23] was found by analyzing the  $\Xi_b^- \rightarrow J/\psi \Lambda K^-$  process, which can be regarded as the  $\Xi_c \bar{D}^*$  molecular candidate [25–34]. Later, LHCb found the  $P_{\psi_s}^\Lambda(4338)$  [24] in the  $J/\psi \Lambda$  invariant mass spectrum of the  $B^- \rightarrow J/\psi \Lambda \bar{p}$  weak de-

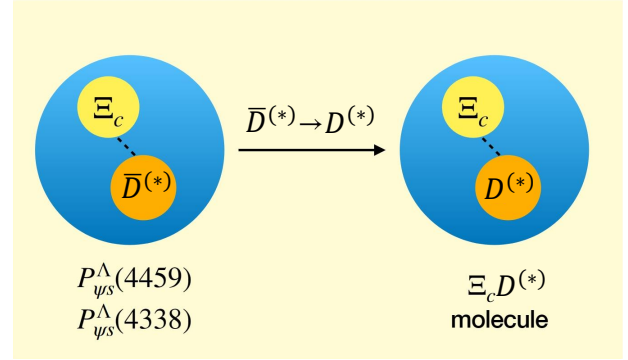


FIG. 1: The  $\Xi_c D^{(*)}$  molecular states are the partners of the  $\Xi_c \bar{D}^{(*)}$  molecular states [25–34] by substituting the  $\bar{D}^{(*)}$  meson with the  $D^{(*)}$  meson.

cay, which can be interpreted as the  $\Xi_c \bar{D}$  molecular candidate [25–34]. Interestingly, the mass gap between the  $P_{\psi_s}^\Lambda(4459)$  and  $P_{\psi_s}^\Lambda(4338)$  states is similar to that of these observed  $p_{\psi}^N$  states [35, 36], showing the possibility of the existence of the double peak structures located just below the threshold of the  $\Xi_c \bar{D}^*$  channel for the  $P_{\psi_s}^\Lambda(4459)$  [35, 36]. It awaits future testing by more accurate data. Having these  $P_{\psi_s}^\Lambda(4459)$  and  $P_{\psi_s}^\Lambda(4338)$  states, we can make an extension as shown in Fig. 1, where  $\bar{D}^{(*)}$  is replaced by  $D^{(*)}$ . This treatment makes us interested in exploring the  $\Xi_c D^{(*)}$  molecular states, which belong to the typical double-charm molecular pentaquark systems.

In fact, the discussed double-charm molecular  $\Xi_c D^{(*)}$  pentaquarks are closely related to the  $T_{cc}(3875)^+$  observed in the  $D^0 D^0 \pi^+$  invariant mass spectrum produced by the  $pp$  collisions [37], which can be explained as the  $DD^*$  molecular

\*Electronic address: wangfl2016@lzu.edu.cn

†Electronic address: xiangliu@lzu.edu.cn

tetraquark candidate [38–49]. As illustrated in Fig. 2, the discussed  $\Xi_c^{(*)}D^{(*)}$  molecular pentaquarks are a logical extension of the  $T_{cc}(3875)^+$  state due to the replacement of  $D \rightarrow \Xi_c^{(*)}$ . Obviously, the study of the  $\Xi_c^{(*)}D^{(*)}$  double-charm molecular pentaquarks can further enrich our knowledge of the double-heavy exotic multiquarks [50–52]. The present work may encourage our experimental colleagues to have ambitions to find out the predicted  $\Xi_c^{(*)}D^{(*)}$  molecular pentaquarks.

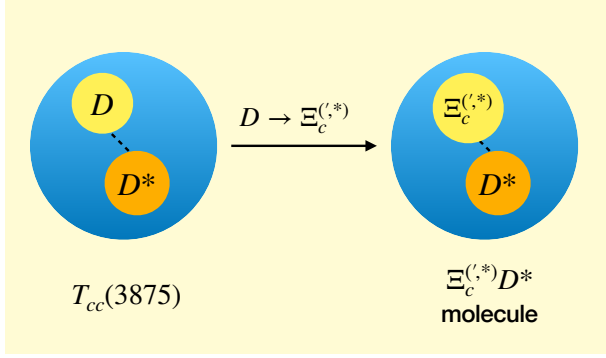


FIG. 2: The investigation of the  $\Xi_c^{(*)}D^{(*)}$  molecular states is a logical extension of the observed  $T_{cc}(3875)^+$  state [37] as the  $DD^*$  molecular tetraquark candidate [38–49].

In this paper, we study the mass spectra and the corresponding spatial wave functions of the  $\Xi_c^{(*)}D^{(*)}$ -type double-charm molecular pentaquark candidates with single strangeness, which are important not only for experimentally searching for these molecular candidates but also for theoretically analyzing their properties. In our concrete analysis, the interactions of the  $\Xi_c^{(*)}D^{(*)}$  systems can be investigated through the one-boson-exchange (OBE) model [4, 9] and take into account both the  $S$ - $D$  wave mixing effect and the coupled channel effect, and the coupled channel Schrödinger equation is then employed to analyze their bound state properties including the binding energies and the spatial wave functions, which is the successful approach to reproduce the bound state properties of the deuteron as the molecular state consisting of the neutron and the proton [4, 40, 53–58]. After that, we investigate the M1 radiative decay behaviors and the magnetic moments of the isoscalar  $\Xi_c^{(*)}D^{(*)}$  molecular states based on the obtained mass spectra and spatial wave functions, which can provide the deeper insights into their inner structures and properties. In our calculations, the constituent quark model is employed, which is the widely accepted method for exploring the electromagnetic properties of the hadronic states [52, 59–104].

The structure of this paper is as follows. In Sec. II, we utilise the OBE model to derive the interactions for the  $\Xi_c^{(*)}D^{(*)}$  systems. Following this, we obtain the mass spectra and the corresponding spatial wave functions of the  $\Xi_c^{(*)}D^{(*)}$ -type double-charm molecular pentaquark candidates with single strangeness. In Sec. III, we investigate the M1 radiative decay behaviors and the magnetic moments of the isoscalar  $\Xi_c^{(*)}D^{(*)}$  molecular states based on the obtained mass spectra and spatial wave functions using the constituent quark model. Finally, a summary is presented in Sec. IV.

## II. THE MASS SPECTRA AND THE CORRESPONDING SPATIAL WAVE FUNCTIONS OF THE DISCUSSED PENTAQUARKS

In this section, we first derive the OBE effective potentials of the  $\Xi_c^{(*)}D^{(*)}$  systems, and then their bound state properties comprising of the binding energies  $E$  and the corresponding spatial wave functions  $\phi(r)$  can be discussed by solving the coupled channel Schrödinger equation, which can provide the essential information for establishing the mass spectra and investigating the properties of the  $\Xi_c^{(*)}D^{(*)}$  molecular pentaquarks.

### A. The OBE effective potentials of the $\Xi_c^{(*)}D^{(*)}$ systems

When analyzing the bound state properties of the  $\Xi_c^{(*)}D^{(*)}$  systems, it is imperative to investigate their interactions. In this study, we utilise the OBE model to explore the interactions of the  $\Xi_c^{(*)}D^{(*)}$  systems, which includes bosons such as the scalar meson  $\sigma$ , the pseudoscalar mesons  $\pi$  and  $\eta$ , as well as the vector mesons  $\rho$  and  $\omega$  [4, 9]. In the concrete calculations, the effective Lagrangian approach is utilized. Thus, it is crucial to construct the effective Lagrangians describing the interactions among the heavy hadrons  $\Xi_c^{(*)}/D^{(*)}$  and the light scalar, pseudoscalar, and vector mesons  $\mathcal{E}$ .

#### 1. Effective Lagrangians concerning the interactions between the heavy hadrons $\Xi_c^{(*)}/D^{(*)}$ and the light mesons $\mathcal{E}$

For the  $S$ -wave single-charmed baryons in the  $6_F$  flavour representation  $\mathcal{B}_6$  and  $\mathcal{B}_6^*$ , it is necessary to construct the superfield  $\mathcal{S}_\mu$  according to the heavy quark spin symmetry [105–111], i.e.,

$$\mathcal{S}_\mu = -\sqrt{\frac{1}{3}}(\gamma_\mu + v_\mu)\gamma^5\mathcal{B}_6 + \mathcal{B}_{6\mu}^*. \quad (2.1)$$

Furthermore, the superfield  $H_a^{(Q)}$  can be formed by utilizing the  $S$ -wave charmed mesons  $D$  with  $J^P = 0^-$  and  $D^*$  with  $J^P = 1^-$ , which can be expressed in the following manner [112]

$$H_a^{(Q)} = \frac{1+\not{v}}{2}(D_a^{*\mu}\gamma_\mu - D_a\gamma_5). \quad (2.2)$$

Here, the four-velocity is represented as  $v_\mu$  and has the value  $v_\mu = (1, 0)$  when making the non-relativistic approximation. In addition, the associated conjugate fields are  $\bar{\mathcal{S}}_\mu = \mathcal{S}_\mu^\dagger\gamma^0$  and  $\bar{H}_a^{(Q)} = \gamma^0 H_a^{(Q)\dagger}\gamma^0$  [105–112]. In the previously defined superfields, the normalization relations for the heavy hadrons  $\mathcal{B}$ ,  $\mathcal{B}^*$ ,  $D$ , and  $D^*$  are expressed as  $\langle 0|\mathcal{B}|cqq(1/2^+)\rangle = \sqrt{2m_{\mathcal{B}}}(\chi_{\frac{1}{2}m}, \frac{\sigma\cdot p}{2m_{\mathcal{B}}}\chi_{\frac{1}{2}m})^T$ ,  $\langle 0|\mathcal{B}^*|cqq(3/2^+)\rangle = \sqrt{2m_{\mathcal{B}^*}}(\Phi_{\frac{3}{2}m}^\mu, \frac{\sigma\cdot p}{2m_{\mathcal{B}^*}}\Phi_{\frac{3}{2}m}^\mu)^T$ ,  $\langle 0|D|c\bar{q}(0^-)\rangle = \sqrt{m_D}$ , and  $\langle 0|D^*|c\bar{q}(1^-)\rangle = \sqrt{m_{D^*}}\epsilon^\mu$  [105–112]. Here, the mass of the heavy hadron  $i$  is  $m_i$ ,

the Pauli matrix of the charmed baryon  $\mathcal{B}^{(*)}$  is  $\sigma$ , and the momentum of the charmed baryon  $\mathcal{B}^{(*)}$  is  $p$ . Within the static limit, the polarization vector  $\epsilon_m^\mu$  ( $m = 0, \pm 1$ ) assumes the values of  $\epsilon_-^\mu = (0, -1, i, 0) / \sqrt{2}$ ,  $\epsilon_0^\mu = (0, 0, 0, -1)$ , and  $\epsilon_+^\mu = (0, 1, i, 0) / \sqrt{2}$ . The spin wave function describing the baryon with the spin of  $S = 1/2$  is represented by  $\chi_{\frac{1}{2}m}$ , the polarization tensor  $\Phi_{\frac{3}{2}m}^\mu$  represents the spin wave function of the baryon with the spin of  $S = 3/2$  and can be represented as  $\Phi_{\frac{3}{2}m}^\mu = \sum_{m_1, m_2} C_{\frac{1}{2}m_1, \frac{1}{2}m_2}^{\frac{3}{2}m} \chi_{\frac{1}{2}m_1} \epsilon_{m_2}^\mu$ , where the constant  $C_{ab,cd}^{ef}$  is the Clebsch-Gordan coefficient.

Utilising the restrictions of the heavy quark symmetry, the chiral symmetry, and the hidden local symmetry [106–110], the effective Lagrangians for the interactions between the heavy hadrons  $\Xi_c^{(*)}/D^{(*)}$  and the light scalar, pseudoscalar, and vector mesons  $\mathcal{E}$  are constructed as [105–112]

$$\mathcal{L}_{\mathcal{B}_3 \mathcal{B}_3 \mathcal{E}} = l_B \langle \bar{\mathcal{B}}_3 \sigma \mathcal{B}_3 \rangle + i\beta_B \langle \bar{\mathcal{B}}_3 v^\mu (\mathcal{V}_\mu - \rho_\mu) \mathcal{B}_3 \rangle, \quad (2.3)$$

$$\begin{aligned} \mathcal{L}_{SSE} = & l_S \langle \bar{S}_\mu \sigma S^\mu \rangle - \frac{3}{2} g_1 \epsilon^{\mu\nu\lambda\kappa} v_\kappa \langle \bar{S}_\mu \mathcal{A}_\nu S_\lambda \rangle \\ & + i\beta_S \langle \bar{S}_\mu v_\alpha (\mathcal{V}^\alpha - \rho^\alpha) S^\mu \rangle + \lambda_S \langle \bar{S}_\mu F^{\mu\nu}(\rho) S_\nu \rangle, \end{aligned} \quad (2.4)$$

$$\mathcal{L}_{\mathcal{B}_3 S \mathcal{E}} = ig_4 \langle \bar{S}_\mu \mathcal{A}_\mu \mathcal{B}_3 \rangle + i\lambda_I \epsilon^{\mu\nu\lambda\kappa} v_\mu \langle \bar{S}_\nu F_{\lambda\kappa} \mathcal{B}_3 \rangle + h.c., \quad (2.5)$$

$$\begin{aligned} \mathcal{L}_{HHE} = & g_\sigma \langle H_a^{(Q)} \sigma \bar{H}_a^{(Q)} \rangle + ig \langle H_b^{(Q)} \mathcal{A}_{ba} \gamma_5 \bar{H}_a^{(Q)} \rangle \\ & + i\beta \langle H_b^{(Q)} v^\mu (\mathcal{V}_\mu - \rho_\mu)_{ba} \bar{H}_a^{(Q)} \rangle \\ & + i\lambda \langle H_b^{(Q)} \sigma^{\mu\nu} F_{\mu\nu}(\rho)_{ba} \bar{H}_a^{(Q)} \rangle. \end{aligned} \quad (2.6)$$

In the effective Lagrangians presented above, we identify the  $S$ -wave charmed baryons in the  $\bar{3}_F$  flavor representation and the  $6_F$  flavor representation as the  $\mathcal{B}_3$  and the  $\mathcal{B}_6^{(*)}$ , which are defined as follows [105–111]

$$\mathcal{B}_3 = \begin{pmatrix} 0 & \Lambda_c^+ & \Xi_c^+ \\ -\Lambda_c^+ & 0 & \Xi_c^0 \\ -\Xi_c^+ & -\Xi_c^0 & 0 \end{pmatrix}, \mathcal{B}_6^{(*)} = \begin{pmatrix} \Sigma_c^{(*)++} & \Sigma_c^{(*)+} & \Xi_c^{(*)+} \\ \Sigma_c^{(*)+} & \Sigma_c^{(*)0} & \Xi_c^{(*)0} \\ \Xi_c^{(*)+} & \Xi_c^{(*)0} & \Omega_c^{(*)0} \end{pmatrix}, \quad (2.7)$$

respectively. The axial current  $\mathcal{A}_\mu$  and the vector current  $\mathcal{V}_\mu$  are

$$\mathcal{A}_\mu = \frac{1}{2} (\xi^\dagger \partial_\mu \xi - \xi \partial_\mu \xi^\dagger), \quad \mathcal{V}_\mu = \frac{1}{2} (\xi^\dagger \partial_\mu \xi + \xi \partial_\mu \xi^\dagger), \quad (2.8)$$

respectively. The pseudo-Goldstone meson field is defined as  $\xi = e^{i\mathbb{P}/f_\pi}$  with  $f_\pi$  being equal to 132 MeV, and the light pseudoscalar meson matrix  $\mathbb{P}$  is [105–112]

$$\mathbb{P} = \begin{pmatrix} \frac{\pi^0}{\sqrt{2}} + \frac{\eta}{\sqrt{6}} & \pi^+ & K^+ \\ \pi^- & -\frac{\pi^0}{\sqrt{2}} + \frac{\eta}{\sqrt{6}} & K^0 \\ K^- & \bar{K}^0 & -\sqrt{\frac{2}{3}}\eta \end{pmatrix}. \quad (2.9)$$

Furthermore, the vector meson field and the vector meson field strength tensor are defined as  $\rho_\mu$  and  $F_{\mu\nu}$ , which can be mathematically expressed as follows

$$\rho_\mu = \frac{ig_V}{\sqrt{2}} \mathbb{V}_\mu, \quad F_{\mu\nu} = \partial_\mu \rho_\nu - \partial_\nu \rho_\mu + [\rho_\mu, \rho_\nu], \quad (2.10)$$

respectively. Here, the light vector meson matrix  $\mathbb{V}_\mu$  is [105–112]

$$\mathbb{V}_\mu = \begin{pmatrix} \frac{\rho^0}{\sqrt{2}} + \frac{\omega}{\sqrt{2}} & \rho^+ & K^{*+} \\ \rho^- & -\frac{\rho^0}{\sqrt{2}} + \frac{\omega}{\sqrt{2}} & K^{*0} \\ K^{*-} & \bar{K}^{*0} & \phi \end{pmatrix}_\mu. \quad (2.11)$$

Following the preceding discussions, we can derive the specific effective Lagrangians illustrating the interactions between the heavy hadrons  $\Xi_c^{(*)}/D^{(*)}$  and the light scalar, pseudoscalar, and vector mesons  $\mathcal{E}$ , which can be achieved by expanding the effective Lagrangians constructed above to the leading order of the pseudo-Goldstone meson field  $\xi$  as explained below

$$\mathcal{L}_{\mathcal{B}_3 \mathcal{B}_3 \sigma} = l_B \langle \bar{\mathcal{B}}_3 \sigma \mathcal{B}_3 \rangle, \quad (2.12)$$

$$\begin{aligned} \mathcal{L}_{\mathcal{B}_6^{(*)} \mathcal{B}_6^{(*)} \sigma} = & -l_S \langle \bar{\mathcal{B}}_6 \sigma \mathcal{B}_6 \rangle + l_S \langle \bar{\mathcal{B}}_6^* \sigma \mathcal{B}_6^{*\mu} \rangle \\ & - \frac{l_S}{\sqrt{3}} \langle \bar{\mathcal{B}}_6^* \sigma (\gamma^\mu + v^\mu) \gamma^5 \mathcal{B}_6 \rangle + h.c., \end{aligned} \quad (2.13)$$

$$\mathcal{L}_{HH\sigma} = -2g_\sigma D_a \sigma D_a^\dagger + 2g_\sigma D_{a\mu}^* \sigma D_a^{*\mu}, \quad (2.14)$$

$$\begin{aligned} \mathcal{L}_{\mathcal{B}_6^{(*)} \mathcal{B}_6^{(*)} \mathbb{P}} = & i \frac{g_1}{2f_\pi} \epsilon^{\mu\nu\lambda\kappa} v_\kappa \langle \bar{\mathcal{B}}_6 \gamma_\mu \gamma_\lambda \partial_\nu \mathbb{P} \mathcal{B}_6 \rangle \\ & - i \frac{3g_1}{2f_\pi} \epsilon^{\mu\nu\lambda\kappa} v_\kappa \langle \bar{\mathcal{B}}_6^* \partial_\nu \mathbb{P} \mathcal{B}_6^* \rangle \\ & + i \frac{\sqrt{3}g_1}{2f_\pi} v_\kappa \epsilon^{\mu\nu\lambda\kappa} \langle \bar{\mathcal{B}}_6^* \partial_\nu \mathbb{P} \gamma_\lambda \gamma^5 \mathcal{B}_6 \rangle + h.c., \end{aligned} \quad (2.15)$$

$$\begin{aligned} \mathcal{L}_{\mathcal{B}_3 \mathcal{B}_6^{(*)} \mathbb{P}} = & -\sqrt{\frac{1}{3}} \frac{g_4}{f_\pi} \langle \bar{\mathcal{B}}_6 \gamma^5 (\gamma^\mu + v^\mu) \partial_\mu \mathbb{P} \mathcal{B}_3 \rangle \\ & - \frac{g_4}{f_\pi} \langle \bar{\mathcal{B}}_6^* \partial^\mu \mathbb{P} \mathcal{B}_3 \rangle + h.c., \end{aligned} \quad (2.16)$$

$$\begin{aligned} \mathcal{L}_{HH\mathbb{P}} = & -\frac{2ig}{f_\pi} v^\alpha \epsilon_{\alpha\mu\nu\lambda} D_b^{*\mu} D_a^{*\lambda\dagger} \partial^\nu \mathbb{P}_{ba} \\ & - \frac{2g}{f_\pi} (D_b^{*\mu} D_a^\dagger + D_b D_a^{*\mu\dagger}) \partial_\mu \mathbb{P}_{ba}, \end{aligned} \quad (2.17)$$

$$\mathcal{L}_{\mathcal{B}_3 \mathcal{B}_3 \mathbb{V}} = \frac{1}{\sqrt{2}} \beta_B g_V \langle \bar{\mathcal{B}}_3 v \cdot \mathbb{V} \mathcal{B}_3 \rangle, \quad (2.18)$$

$$\begin{aligned} \mathcal{L}_{\mathcal{B}_6^{(*)} \mathcal{B}_6^{(*)} \mathbb{V}} = & -\frac{\beta_S g_V}{\sqrt{2}} \langle \bar{\mathcal{B}}_6 v \cdot \mathbb{V} \mathcal{B}_6 \rangle + \frac{\beta_S g_V}{\sqrt{2}} \langle \bar{\mathcal{B}}_6^* v \cdot \mathbb{V} \mathcal{B}_6^{*\mu} \rangle \\ & - i \frac{\lambda_S g_V}{3\sqrt{2}} \langle \bar{\mathcal{B}}_6 \gamma_\mu \gamma_\nu (\partial^\mu \mathbb{V}^\nu - \partial^\nu \mathbb{V}^\mu) \mathcal{B}_6 \rangle \\ & + i \frac{\lambda_S g_V}{\sqrt{2}} \langle \bar{\mathcal{B}}_6^* (\partial^\mu \mathbb{V}^\nu - \partial^\nu \mathbb{V}^\mu) \mathcal{B}_6^* \rangle \\ & - i \frac{\lambda_S g_V}{\sqrt{6}} \langle \bar{\mathcal{B}}_6^* (\partial^\mu \mathbb{V}^\nu - \partial^\nu \mathbb{V}^\mu) (\gamma_\nu + v_\nu) \gamma^5 \mathcal{B}_6 \rangle \\ & - \frac{\beta_S g_V}{\sqrt{6}} \langle \bar{\mathcal{B}}_6^* v \cdot \mathbb{V} (\gamma^\mu + v^\mu) \gamma^5 \mathcal{B}_6 \rangle + h.c., \end{aligned} \quad (2.19)$$

$$\begin{aligned} \mathcal{L}_{\mathcal{B}_3 \mathcal{B}_6^{(*)} \mathbb{V}} = & -\frac{\lambda_I g_V}{\sqrt{2}} \epsilon^{\mu\nu\lambda\kappa} v_\mu \langle \bar{\mathcal{B}}_6^* (\partial_\lambda \mathbb{V}_\kappa - \partial_\kappa \mathbb{V}_\lambda) \mathcal{B}_3 \rangle \\ & - \frac{\lambda_I g_V}{\sqrt{6}} \epsilon^{\mu\nu\lambda\kappa} v_\mu \langle \bar{\mathcal{B}}_6^* \gamma^5 \gamma_\nu (\partial_\lambda \mathbb{V}_\kappa - \partial_\kappa \mathbb{V}_\lambda) \mathcal{B}_3 \rangle + h.c., \end{aligned} \quad (2.20)$$

$$\begin{aligned}
\mathcal{L}_{HHV} = & -\sqrt{2}\beta g_V D_b D_a^\dagger v \cdot \nabla_{ba} + \sqrt{2}\beta g_V D_{b\mu}^* D_a^{*\mu\dagger} v \cdot \nabla_{ba} \\
& -2\sqrt{2}i\lambda g_V D_b^* D_a^{*\nu\dagger} (\partial_\mu \nabla_\nu - \partial_\nu \nabla_\mu)_{ba} \\
& -2\sqrt{2}\lambda g_V v^\lambda \varepsilon_{\lambda\mu\alpha\beta} (D_b D_a^{*\mu\dagger} + D_b^* D_a^\dagger) \partial^\alpha \nabla^\beta_{ba}. \quad (2.21)
\end{aligned}$$

The above effective Lagrangians contain several coupling constants to depict the interaction strengths between the heavy hadrons  $\Xi_c^{(\prime,*)}/D^{(*)}$  and the light scalar, pseudoscalar, and vector mesons  $\mathcal{E}$ , and we can estimate these coupling constants by either matching the experimental data or taking the theoretical models. In addition, the phase factors between the relevant coupling constants can then be estimated by applying the quark model [113]. In the subsequent numerical analysis, we take the coupling constants utilized in the present work as  $l_B = -3.65$ ,  $l_S = 6.20$ ,  $g_\sigma = 0.76$ ,  $g_1 = 0.94$ ,  $g_4 = 1.06$ ,  $g = -0.59$ ,  $\beta_{BGV} = -6.00$ ,  $\beta_{SGV} = 10.14$ ,  $\beta_{GV} = -5.25$ ,  $\lambda_{IGV} = -6.80 \text{ GeV}^{-1}$ ,  $\lambda_{SGV} = 19.20 \text{ GeV}^{-1}$ , and  $\lambda_{GV} = -3.27 \text{ GeV}^{-1}$  [36, 51, 52, 58, 111, 114–124]. The relevant masses of the mesons and the baryons used in this work were acquired from the Particle Data Group [125], and we utilise  $m_\sigma = 600.00 \text{ MeV}$ ,  $m_\pi = 137.27 \text{ MeV}$ ,  $m_\eta = 547.86 \text{ MeV}$ ,  $m_\rho = 775.26 \text{ MeV}$ ,  $m_\omega = 782.66 \text{ MeV}$ ,  $m_{\Xi_c^+} = 2467.71 \text{ MeV}$ ,  $m_{\Xi_c^0} = 2470.44 \text{ MeV}$ ,  $m_{\Xi_c^{*+}} = 2578.20 \text{ MeV}$ ,  $m_{\Xi_c^{*0}} = 2578.70 \text{ MeV}$ ,  $m_{\Xi_c^{*+}} = 2645.10 \text{ MeV}$ ,  $m_{\Xi_c^{*0}} = 2645.16 \text{ MeV}$ ,  $m_{D^+} = 1869.66 \text{ MeV}$ ,  $m_{D^0} = 1864.84 \text{ MeV}$ ,  $m_{D^{*+}} = 2006.85 \text{ MeV}$ , and  $m_{D^{*0}} = 2010.26 \text{ MeV}$  [125].

## 2. How to derive the OBE effective potentials for the $\Xi_c^{(\prime,*)}D^{(*)}$ systems

In the following, we demonstrate the deduction of the OBE effective potentials for the  $\Xi_c^{(\prime,*)}D^{(*)}$  systems by utilizing the constructed effective Lagrangians [105–112]. By referring to the obtained effective Lagrangians, we can determine the scattering amplitude  $\mathcal{M}_{\Xi_c^{(\prime,*)}D^{(*)} \rightarrow \Xi_c^{(\prime,*)}D^{(*)}}(q)$  for the  $\Xi_c^{(\prime,*)}D^{(*)} \rightarrow \Xi_c^{(\prime,*)}D^{(*)}$  process. And then, we adopt both the Breit approximation and the non-relativistic normalization to extract the effective potential in the momentum space  $\mathcal{V}_E^{\Xi_c^{(\prime,*)}D^{(*)} \rightarrow \Xi_c^{(\prime,*)}D^{(*)}}(q)$  using the following equation [126]

$$\mathcal{V}_E^{\Xi_c^{(\prime,*)}D^{(*)} \rightarrow \Xi_c^{(\prime,*)}D^{(*)}}(q) = -\frac{\mathcal{M}_{\Xi_c^{(\prime,*)}D^{(*)} \rightarrow \Xi_c^{(\prime,*)}D^{(*)}}(q)}{\sqrt{2m_{\Xi_c^{(\prime,*)}}2m_{D^{(*)}}2m_{\Xi_c^{(\prime,*)}}2m_{D^{(*)}}}} \quad (2.22)$$

Finally, we can calculate the effective potential in the coordinate space  $\mathcal{V}_E^{\Xi_c^{(\prime,*)}D^{(*)} \rightarrow \Xi_c^{(\prime,*)}D^{(*)}}(r)$  by utilizing the Fourier transformation for the effective potential in the momentum space  $\mathcal{V}_E^{\Xi_c^{(\prime,*)}D^{(*)} \rightarrow \Xi_c^{(\prime,*)}D^{(*)}}(q)$  along with the form factor  $\mathcal{F}(q^2, m_\mathcal{E}^2)$  [4, 9], i.e.,

$$\begin{aligned}
& \mathcal{V}_E^{\Xi_c^{(\prime,*)}D^{(*)} \rightarrow \Xi_c^{(\prime,*)}D^{(*)}}(r) \\
& = \int \frac{d^3q}{(2\pi)^3} e^{iq \cdot r} \mathcal{V}_E^{\Xi_c^{(\prime,*)}D^{(*)} \rightarrow \Xi_c^{(\prime,*)}D^{(*)}}(q) \mathcal{F}^2(q^2, m_\mathcal{E}^2) \quad (2.23)
\end{aligned}$$

Here, we have included the form factor  $\mathcal{F}(q^2, m_\mathcal{E}^2)$  at two interaction vertices in the Feynman diagram to account for the

inner structures of the discussed hadrons and the off-shell nature of the exchanged light mesons. Similar to the study of the bound state properties of the deuteron [4, 40, 53–58], we select the monopole-type form factor  $\mathcal{F}(q^2, m_\mathcal{E}^2) = (\Lambda^2 - m_\mathcal{E}^2)/(\Lambda^2 - q^2)$  in this work, where  $\Lambda$  represents the cut-off parameter, and the four momentum and the mass of the exchanged light meson are defined as  $q$  and  $m_\mathcal{E}$ , respectively.

For the  $\Xi_c^{(\prime,*)}D^{(*)}$  systems, the flavour wave functions  $|I, m_I\rangle$  can be constructed as

$$\begin{aligned}
|1, 1\rangle &= |\Xi_c^{(\prime,*)+} D^{(*)+}\rangle, \\
|1, 0\rangle &= -\sqrt{\frac{1}{2}} |\Xi_c^{(\prime,*)+} D^{(*)0}\rangle + \sqrt{\frac{1}{2}} |\Xi_c^{(\prime,*)0} D^{(*)+}\rangle, \\
|1, -1\rangle &= -|\Xi_c^{(\prime,*)0} D^{(*)0}\rangle, \\
|0, 0\rangle &= -\sqrt{\frac{1}{2}} |\Xi_c^{(\prime,*)+} D^{(*)0}\rangle - \sqrt{\frac{1}{2}} |\Xi_c^{(\prime,*)0} D^{(*)+}\rangle,
\end{aligned}$$

where the isospins and the corresponding third components of the  $\Xi_c^{(\prime,*)}D^{(*)}$  systems are denoted as the symbols  $I$  and  $m_I$ , respectively. And then, we provide the information on the spin-orbital wave functions  $|^{2S+1}L_J\rangle$  for the  $\Xi_c^{(\prime,*)}D^{(*)}$  systems as follows

$$\begin{aligned}
\Xi_c^{(\prime)}D &: |^{2S+1}L_J\rangle = \sum_{m, m_L} C_{\frac{1}{2}m, Lm_L}^{JM} \chi_{\frac{1}{2}m} Y_{Lm_L}, \\
\Xi_c^*D &: |^{2S+1}L_J\rangle = \sum_{m, m_L} C_{\frac{3}{2}m, Lm_L}^{JM} \Phi_{\frac{3}{2}m} Y_{Lm_L}, \\
\Xi_c^{(\prime)}D^* &: |^{2S+1}L_J\rangle = \sum_{m, m', m_S, m_L} C_{\frac{1}{2}m, 1m'}^{S m_S} C_{S m_S, Lm_L}^{JM} \chi_{\frac{1}{2}m} \epsilon_{m'}^\mu Y_{Lm_L}, \\
\Xi_c^*D^* &: |^{2S+1}L_J\rangle = \sum_{m, m', m_S, m_L} C_{\frac{3}{2}m, 1m'}^{S m_S} C_{S m_S, Lm_L}^{JM} \Phi_{\frac{3}{2}m}^\mu \epsilon_{m'}^\nu Y_{Lm_L},
\end{aligned}$$

where the spin, the orbital angular momentum, and the total angular momentum for the  $\Xi_c^{(\prime,*)}D^{(*)}$  systems are denoted by the symbols  $S$ ,  $L$ , and  $J$  within the spin-orbital wave functions  $|^{2S+1}L_J\rangle$ , respectively. Furthermore, the spherical harmonic function is denoted by  $Y_{Lm_L}$ .

Given the unique impacts of the  $S$ - $D$  wave mixing effect and the coupled channel effect in the discussion of the  $\Xi_c^{(\prime)}\bar{D}^{(*)}$  molecular states [36], it is imperative to consider the contribution of the  $S$ - $D$  wave mixing effect and the coupled channel effect when studying the bound state properties of the  $\Xi_c^{(\prime,*)}D^{(*)}$  systems. The  $S$ -wave and  $D$ -wave channels  $|^{2S+1}L_J\rangle$  for the  $\Xi_c^{(\prime,*)}D^{(*)}$  systems are detailed below

- $\Xi_c^{(\prime)}D$  system:

$$J^P = \frac{1}{2}^- : |^2\mathbb{S}_{\frac{1}{2}}\rangle,$$

- $\Xi_c^*D$  system:

$$J^P = \frac{3}{2}^- : |^4\mathbb{S}_{\frac{3}{2}}\rangle, |^4\mathbb{D}_{\frac{3}{2}}\rangle,$$



- $\Xi_c^{(\prime)}D^*$  system:

$$J^P = \frac{1}{2}^- : \left| {}^2\mathbb{S}_{\frac{1}{2}} \right\rangle, \left| {}^4\mathbb{D}_{\frac{1}{2}} \right\rangle$$

$$J^P = \frac{3}{2}^- : \left| {}^4\mathbb{S}_{\frac{3}{2}} \right\rangle, \left| {}^2\mathbb{D}_{\frac{3}{2}} \right\rangle, \left| {}^4\mathbb{D}_{\frac{3}{2}} \right\rangle,$$

- $\Xi_c^*D^*$  system:

$$J^P = \frac{1}{2}^- : \left| {}^2\mathbb{S}_{\frac{1}{2}} \right\rangle, \left| {}^4\mathbb{D}_{\frac{1}{2}} \right\rangle, \left| {}^6\mathbb{D}_{\frac{1}{2}} \right\rangle$$

$$J^P = \frac{3}{2}^- : \left| {}^4\mathbb{S}_{\frac{3}{2}} \right\rangle, \left| {}^2\mathbb{D}_{\frac{3}{2}} \right\rangle, \left| {}^4\mathbb{D}_{\frac{3}{2}} \right\rangle, \left| {}^6\mathbb{D}_{\frac{3}{2}} \right\rangle$$

$$J^P = \frac{5}{2}^- : \left| {}^6\mathbb{S}_{\frac{5}{2}} \right\rangle, \left| {}^2\mathbb{D}_{\frac{5}{2}} \right\rangle, \left| {}^4\mathbb{D}_{\frac{5}{2}} \right\rangle, \left| {}^6\mathbb{D}_{\frac{5}{2}} \right\rangle.$$

Here, the spin  $S$ , the orbital angular momentum  $L$ , and the total angular momentum  $J$  of the relevant channels are denoted by the notation  $|^{2S+1}L_J\rangle$ . In addition, we take the symbols  $L = \mathbb{S}$  and  $\mathbb{D}$  to stand for the interactions in the corresponding  $S$ -wave and  $D$ -wave channels, respectively.

The above procedure can be employed to calculate the OBE effective potentials in the coordinate space for the  $\Xi_c^{(\prime,*)}D^{(*)}$  systems [36, 52, 58, 114, 116–121, 123, 127]. Based on the effective potentials in the coordinate space for the  $\Xi_c^{(\prime,*)}D^{(*)}$  systems obtained through the OBE model, the coupled channel Schrödinger equation enables us to discuss the binding energies  $E$  and the spatial wave functions  $\phi(r)$  for the  $\Xi_c^{(\prime,*)}D^{(*)}$  systems. In addition, the aforementioned spatial wave functions  $\phi(r)$  enable us to compute the root-mean-square radius  $r_{\text{RMS}}$  and the individual channel probabilities  $P_i$ . These parameters can offer the valuable guidance in establishing the mass spectra and investigating the properties of the  $\Xi_c^{(\prime,*)}D^{(*)}$ -type double-charm molecular pentaquark candidates with single strangeness. In the realistic calculations, we search for the loosely bound state solutions for the  $\Xi_c^{(\prime,*)}D^{(*)}$  systems by varying the cutoff parameter within the range of 0.8 to 2.0 GeV, and the reasonable input for discussing the hadronic molecular states is the cutoff parameter about 1.0 GeV in the monopole-type form factor, which is based on previous experiences studying the deuteron's bound state properties within the OBE model [4, 40, 53–58]. Considering that the hadronic molecular state is the loosely bound state comprising the hadrons, the most promising hadronic molecular candidate should have the small binding energy and the large size to avoid the excessive overlap between the corresponding constituent hadrons in their spatial distribution [4, 111].

### B. The mass spectra and the corresponding spatial wave functions of the $\Xi_c^{(\prime,*)}D^{(*)}$ molecular pentaquarks

In the following, we analyze the bound state properties of the  $\Xi_c^{(\prime,*)}D^{(*)}$  systems by considering the  $S$ - $D$  wave mixing effect and the coupled channel effect, which enables us to obtain the mass spectra and the corresponding spatial wave functions for the  $\Xi_c^{(\prime,*)}D^{(*)}$  molecular states.

#### 1. $\Xi_c D$ system

In Table I, we list the bound state properties for the  $\Xi_c D$  state with  $I(J^P) = 0(1/2^-)$  revealed by both the single channel analysis and the coupled channel analysis.

TABLE I: The obtained bound state solutions for the  $\Xi_c D$  state with  $I(J^P) = 0(1/2^-)$ . The cutoff parameter  $\Lambda$ , binding energy  $E$ , and root-mean-square radius  $r_{\text{RMS}}$  are measured in units of GeV, MeV, and fm, respectively. It is worth mentioning that the primary probability of the corresponding channels is emphasized in bold font.

Single channel analysis			
$\Lambda$	$E$	$r_{\text{RMS}}$	
1.18	-0.28	4.97	
1.28	-4.80	1.67	
1.37	-12.85	1.12	
Coupled channel analysis			
$\Lambda$	$E$	$r_{\text{RMS}}$	$P(\Xi_c D / \Xi_c' D / \Xi_c D^* / \Xi_c' D^* / \Xi_c^* D^*)$
1.01	-0.27	4.93	<b>98.12</b> /0.02/0.04/0.97/0.86
1.04	-3.24	1.84	<b>90.96</b> /0.26/0.61/5.30/2.86
1.07	-13.36	0.81	<b>53.79</b> /4.49/13.08/27.63/1.00

By performing the single channel analysis, the isoscalar  $\Xi_c D$  state with  $J^P = 1/2^-$  displays the loosely bound state solutions when the cutoff value  $\Lambda$  exceeds 1.18 GeV. Furthermore, the bound state properties for the  $\Xi_c D$  state with  $I(J^P) = 0(1/2^-)$  can also be explored by taking into account the coupled channel effect involving the  $\Xi_c D$ ,  $\Xi_c' D$ ,  $\Xi_c D^*$ ,  $\Xi_c' D^*$ , and  $\Xi_c^* D^*$  channels. By numerically solving the coupled channel Schrödinger equation, the loosely bound state solutions can be obtained for the  $\Xi_c D$  state with  $I(J^P) = 0(1/2^-)$  when the cutoff value  $\Lambda$  is greater than 1.01 GeV, where the primary contributor is the  $\Xi_c D$  channel. As the cutoff parameter increases, the binding energy of the  $\Xi_c D$  state with  $I(J^P) = 0(1/2^-)$  increases, and other channels such as the  $\Xi_c D^*$  and  $\Xi_c' D^*$  become increasingly significant. In conclusion, the  $\Xi_c D$  state with  $I(J^P) = 0(1/2^-)$  can be regarded as the ideal candidate of the double-charm molecular pentaquark with single strangeness, which can be deemed as the partner of the  $\Xi_c \bar{D}$  molecular state with  $I(J^P) = 0(1/2^-)$  [36]. Subsequent experimental exploration of the  $\Xi_c D$  molecular state with  $I(J^P) = 0(1/2^-)$  can potentially clarify the explanation of the observed  $P_{\psi\psi}^\Lambda(4338)$  state [24] as the  $\Xi_c \bar{D}$  molecular state with  $I(J^P) = 0(1/2^-)$  [25–34].

For the  $\Xi_c D$  state with  $I(J^P) = 1(1/2^-)$ , our analysis indicates that it fails to exhibit the loosely bound state solutions when varying the cutoff parameter between 0.8 to 2.0 GeV even after increasing the contribution of the coupled channel effect. Consequently, it is not recommended to consider the  $\Xi_c D$  state with  $I(J^P) = 1(1/2^-)$  as the candidate of the double-charm molecular pentaquark with single strangeness.

## 2. $\Xi'_c D$ system

In Table II, we present the bound state properties for the  $\Xi'_c D$  state with  $I(J^P) = 0(1/2^-)$ , where we conducted both the single channel analysis and the coupled channel analysis.

TABLE II: The obtained bound state solutions for the  $\Xi'_c D$  state with  $I(J^P) = 0(1/2^-)$ . The cutoff parameter  $\Lambda$ , binding energy  $E$ , and root-mean-square radius  $r_{\text{RMS}}$  are measured in units of GeV, MeV, and fm, respectively. It is worth noting that the primary probability of the corresponding channels is highlighted in bold font.

Single channel analysis			
$\Lambda$	$E$	$r_{\text{RMS}}$	
1.24	-0.25	5.10	
1.36	-4.72	1.66	
1.47	-12.81	1.10	
Coupled channel analysis			
$\Lambda$	$E$	$r_{\text{RMS}}$	$P(\Xi'_c D/\Xi_c D^*/\Xi'_c D^*/\Xi_c D^*)$
0.89	-0.61	3.61	<b>86.51</b> /9.61/3.09/0.78
0.92	-6.26	1.19	<b>62.84</b> /25.50/9.34/2.32
0.94	-12.83	0.86	<b>51.90</b> /31.89/13.01/3.20

During the single channel analysis, the  $\Xi'_c D$  state with  $I(J^P) = 0(1/2^-)$  exhibits the loosely bound state solutions if the cutoff parameter exceeds 1.24 GeV. Accounting for the coupled channel effect and considering the cutoff parameter greater than 0.89 GeV, the  $\Xi'_c D$  state with  $I(J^P) = 0(1/2^-)$  exists the loosely bound state solutions. The  $\Xi'_c D$  channel contributes significantly, and the  $\Xi_c D^*$  and  $\Xi'_c D^*$  channels also play the important roles when the  $\Xi'_c D$  state with  $I(J^P) = 0(1/2^-)$  exhibits the larger bound energy. Consequently, we propose the  $\Xi'_c D$  state with  $I(J^P) = 0(1/2^-)$  as the promising candidate of the double-charm molecular pentaquark with single strangeness.

When the cutoff parameter ranges from 0.8 to 2.0 GeV, the  $\Xi'_c D$  state with  $I(J^P) = 1(1/2^-)$  does not emerge the loosely bound state solutions, even if the coupled channel effect is taken into account. Thus, we cannot recommend the  $\Xi'_c D$  state with  $I(J^P) = 1(1/2^-)$  as the candidate of the double-charm molecular pentaquark with single strangeness.

## 3. $\Xi_c D^*$ system

It is well known that the  $P_{\psi s}^\Lambda(4459)$  state [23] can be associated with the  $\Xi_c \bar{D}^*$  molecular candidate [25–34], the study of the  $\Xi_c D^*$  molecular states can enhance the understanding of the inner structure of the  $P_{cs}(4459)$  [35, 36]. In Table III, the bound state solutions for the  $\Xi_c D^*$  system are summarised.

For the single channel analysis, the  $\Xi_c D^*$  states with  $I(J^P) = 0(1/2^-, 3/2^-)$  can form the loosely bound states when the cutoff parameter is greater than 1.17 GeV. If the cutoff parameters are identical, the  $\Xi_c D^*$  states with

TABLE III: The obtained bound state solutions for the  $\Xi_c D^*$  system. The cutoff parameter  $\Lambda$ , binding energy  $E$ , and root-mean-square radius  $r_{\text{RMS}}$  are measured in units of GeV, MeV, and fm, respectively. Notably, the primary probability of the corresponding channels is emphasized in bold font.

$I(J^P)$	Bound state solutions			
$0(1/2^-)$	Single channel analysis			
	$\Lambda$	$E$	$r_{\text{RMS}}$	
	1.17	-0.38	4.57	
	1.26	-4.57	1.68	
	1.35	-12.71	1.11	
	$S$ - $D$ wave mixing analysis			
	$\Lambda$	$E$	$r_{\text{RMS}}$	$P(^2S_{1/2}/^4D_{1/2})$
	1.17	-0.38	4.57	<b>100.00</b> / $o(0)$
	1.26	-4.57	1.68	<b>100.00</b> / $o(0)$
	1.35	-12.71	1.11	<b>100.00</b> / $o(0)$
$0(3/2^-)$	Coupled channel analysis			
	$\Lambda$	$E$	$r_{\text{RMS}}$	$P(\Xi_c D^*/\Xi'_c D^*/\Xi_c D^*)$
	0.94	-0.30	4.70	<b>96.67</b> /2.79/0.54
	0.96	-3.92	1.61	<b>87.54</b> /10.56/1.90
	0.98	-11.92	0.96	<b>78.00</b> /18.79/3.21
	Single channel analysis			
	$\Lambda$	$E$	$r_{\text{RMS}}$	
	1.17	-0.38	4.57	
	1.26	-4.57	1.68	
	1.35	-12.71	1.11	
	$S$ - $D$ wave mixing analysis			
	$\Lambda$	$E$	$r_{\text{RMS}}$	$P(^4S_{3/2}/^2D_{3/2}/^4D_{3/2})$
	1.17	-0.38	4.57	<b>100.00</b> / $o(0)$ / $o(0)$
	1.26	-4.57	1.68	<b>100.00</b> / $o(0)$ / $o(0)$
	1.35	-12.71	1.11	<b>100.00</b> / $o(0)$ / $o(0)$
	Coupled channel analysis			
	$\Lambda$	$E$	$r_{\text{RMS}}$	$P(\Xi_c D^*/\Xi'_c D/\Xi'_c D^*/\Xi_c D^*)$
	0.88	-0.33	4.57	<b>93.92</b> /4.19/0.18/1.72
	0.91	-4.47	1.50	<b>80.82</b> /12.14/0.73/6.31
	0.94	-13.23	0.93	<b>71.61</b> /15.86/1.45/11.08

$I(J^P) = 0(1/2^-, 3/2^-)$  exhibit the comparable binding properties, which can be attributed to the same interaction described by the OBE model for both states in the single channel analysis. For the  $\Xi_c D^*$  states with  $I(J^P) = 0(1/2^-, 3/2^-)$ , we can also analyze the impact of the  $S$ - $D$  wave mixing effect for their bound state properties. Nevertheless, the interactions of the  $\Xi_c D^*$  system do not exist the tensor interac-

tions. Therefore, the  $S$ - $D$  wave mixing effect does not influence the bound state properties for the  $\Xi_c D^*$  states with  $I(J^P) = 0(1/2^-, 3/2^-)$ , where the contribution of the corresponding  $D$ -wave channels is zero. In conclusion, the  $\Xi_c D^*$  states with  $I(J^P) = 0(1/2^-, 3/2^-)$  can be considered as the ideal candidates of the double-charm molecular pentaquarks with single strangeness, and their binding properties are identical when the corresponding cutoff parameters are equal following the single channel analysis and the  $S$ - $D$  wave mixing analysis, which is similar to the bound state properties of the  $\Xi_c \bar{D}^*$  molecular states with  $I(J^P) = 0(1/2^-, 3/2^-)$  [36].

In order to investigate the bound state properties of the  $\Xi_c D^*$  states with  $I(J^P) = 0(1/2^-, 3/2^-)$ , it is essential to take into account the influence of the coupled channel effect, except for the  $S$ - $D$  wave mixing effect. Regarding the  $\Xi_c D^*$  state with  $I(J^P) = 0(1/2^-)$ , the coupling between the  $\Xi_c D^*$ ,  $\Xi'_c D^*$ , and  $\Xi_c^* D^*$  channels can be taken into account, and the loosely bound state solutions arise when the cutoff parameter is set to 0.94 GeV, where the main contribution is provided by the  $\Xi_c D^*$  channel, with the  $\Xi'_c D^*$  and  $\Xi_c^* D^*$  channels also playing the role. For the  $\Xi_c D^*$  state with  $I(J^P) = 0(3/2^-)$ , the coupling of the  $\Xi_c D^*$ ,  $\Xi'_c D^*$ , and  $\Xi_c^* D^*$  channels may affect its binding properties. When setting the cutoff parameter to 0.88 GeV, the  $\Xi_c D^*$  state with  $I(J^P) = 0(3/2^-)$  begins to appear the loosely bound state solutions, and the  $\Xi_c D^*$  channel is the principal contributor, with the  $\Xi'_c D^*$  and  $\Xi_c^* D^*$  channels playing a more significant role as the binding energy increases. By introducing the coupled channel effect, the  $\Xi_c D^*$  states with  $I(J^P) = 0(1/2^-, 3/2^-)$  exhibit different binding properties when both states take the same cutoff parameter, which is analogous to the bound state properties of the  $\Xi_c \bar{D}^*$  molecular states with  $I(J^P) = 0(1/2^-, 3/2^-)$  [36]. Therefore, this proposal suggests that the upcoming experiments should investigate the  $\Xi_c D^*$  molecular states with  $I(J^P) = 0(1/2^-, 3/2^-)$ , which can provide the crucial check for the double peak structures of the  $P_{\psi_s}^\Lambda(4459)$  state [35, 36].

In addition to the  $\Xi_c D^*$  states with  $I(J^P) = 0(1/2^-, 3/2^-)$ , we also examine the bound state properties of the  $\Xi_c D^*$  states with  $I(J^P) = 1(1/2^-, 3/2^-)$ . Unfortunately, the cutoff parameter varies between 0.8 to 2.0 GeV, there is no evidence of the existence of the bound state solutions for the  $\Xi_c D^*$  states with  $I(J^P) = 1(1/2^-, 3/2^-)$  despite the increase in the  $S$ - $D$  wave mixing effect and the coupled channel effect. Hence, the  $\Xi_c D^*$  states with  $I(J^P) = 1(1/2^-, 3/2^-)$  cannot be deemed as the candidates of the double-charm molecular pentaquarks with single strangeness.

#### 4. $\Xi_c D^*$ system

In Table IV, we present the bound state properties for the  $\Xi_c D^*$  state with  $I(J^P) = 0(3/2^-)$ . Here, we need to mention that there are no loosely bound state solutions for the  $\Xi_c D^*$  state with  $I(J^P) = 1(3/2^-)$  when the cutoff parameter variations ranging between 0.8 to 2.0 GeV, despite an increase in the  $S$ - $D$  wave mixing effect and the coupled channel effect. As a result, this rules out the  $\Xi_c D^*$  state with  $I(J^P) = 1(3/2^-)$  as the candidate of the double-charm molecular pentaquark

with single strangeness.

TABLE IV: The obtained bound state solutions for the  $\Xi_c D^*$  state with  $I(J^P) = 0(3/2^-)$ . The cutoff parameter  $\Lambda$ , binding energy  $E$ , and root-mean-square radius  $r_{\text{RMS}}$  are measured in units of GeV, MeV, and fm, respectively. It should be emphasized that the primary probability of the corresponding channels is highlighted in bold font.

Single channel analysis			
$\Lambda$	$E$	$r_{\text{RMS}}$	
1.24	-0.33	4.78	
1.35	-4.45	1.70	
1.46	-12.48	1.11	
$S$ - $D$ wave mixing analysis			
$\Lambda$	$E$	$r_{\text{RMS}}$	$P(^4\mathbb{S}_{\frac{3}{2}}/^4\mathbb{D}_{\frac{3}{2}})$
1.24	-0.33	4.78	<b>100.00</b> / $o(0)$
1.35	-4.45	1.70	<b>100.00</b> / $o(0)$
1.46	-12.48	1.11	<b>100.00</b> / $o(0)$
Coupled channel analysis			
$\Lambda$	$E$	$r_{\text{RMS}}$	$P(\Xi_c^* D / \Xi'_c D^* / \Xi_c D^*)$
1.17	-0.25	5.04	<b>98.84</b> /0.04/1.12
1.21	-1.54	2.62	<b>94.82</b> /0.45/4.73
1.25	-7.70	1.01	<b>51.20</b> /9.44/39.36

When the cutoff parameter is set to 1.24 GeV during the single channel analysis, the  $\Xi_c D^*$  state with  $I(J^P) = 0(3/2^-)$  emerges the loosely bound state solutions. Similar to the  $\Xi_c D$  and  $\Xi'_c D$  systems, the interaction of the  $\Xi_c D^*$  system lacks the tensor interaction. As a result, both the single channel analysis and the  $S$ - $D$  wave mixing analysis can give the same bound state solutions for the  $\Xi_c D^*$  state with  $I(J^P) = 0(3/2^-)$  when the cutoff parameter takes the same value, and the contribution from the  $D$ -wave channel is absent. Furthermore, the coupled channel effect including the  $\Xi_c^* D$ ,  $\Xi'_c D^*$ , and  $\Xi_c D^*$  channels also affect the bound state properties of the  $\Xi_c D^*$  state with  $I(J^P) = 0(3/2^-)$ . When the cutoff parameter is 1.17 GeV, the  $\Xi_c D^*$  state with  $I(J^P) = 0(3/2^-)$  appears the loosely bound state solutions. When the binding energy is shallow, the  $\Xi_c D^*$  channel dominates, but the contribution of the  $\Xi_c^* D^*$  channel increases gradually with the binding energy. Consequently, the  $\Xi_c D^*$  state with  $I(J^P) = 0(3/2^-)$  is suggested as the preferred candidate of the double-charm molecular pentaquark with single strangeness.

#### 5. $\Xi'_c D^*$ system

In Table V, the bound state properties of the  $\Xi'_c D^*$  system are presented, where the influences of the  $S$ - $D$  wave mixing effect and the coupled channel effect are analyzed. When varying the cutoff parameter between 0.8 to 2.0 GeV, the  $\Xi'_c D^*$  states with  $I(J^P) = 1(1/2^-, 3/2^-)$  fail to generate the loosely

bound state solutions, even though the realistic calculations have taken into account several effects like the  $S$ - $D$  wave mixing effect and the coupled channel effect. Thus, the  $\Xi'_c D^*$  states with  $I(J^P) = 1(1/2^-, 3/2^-)$  are not supported as the candidates of the double-charm molecular pentaquarks with single strangeness.

TABLE V: The obtained bound state solutions for the  $\Xi'_c D^*$  system. The cutoff parameter  $\Lambda$ , binding energy  $E$ , and root-mean-square radius  $r_{\text{RMS}}$  are expressed in units of GeV, MeV, and fm, respectively. Emphasis is added in bold to highlight the primary probability of the corresponding channels.

$I(J^P)$	Bound state solutions			
$0(\frac{1}{2}^-)$	Single channel analysis			
	$\Lambda$	$E$	$r_{\text{RMS}}$	
	0.92	-0.66	3.62	
	0.96	-4.94	1.52	
	1.00	-13.74	0.99	
	$S$ - $D$ wave mixing analysis			
	$\Lambda$	$E$	$r_{\text{RMS}}$	$P(^2\mathbb{S}_{\frac{1}{2}}/^4\mathbb{D}_{\frac{1}{2}})$
	0.91	-0.53	3.96	<b>99.67</b> /0.33
	0.95	-4.21	1.64	<b>99.55</b> /0.45
	0.99	-12.03	1.06	<b>99.60</b> /0.40
	Coupled channel analysis			
	$\Lambda$	$E$	$r_{\text{RMS}}$	$P(\Xi'_c D^*/\Xi_c^* D^*)$
$0(\frac{3}{2}^-)$	0.90	-0.63	3.67	<b>98.85</b> /1.15
	0.93	-4.15	1.60	<b>95.91</b> /4.09
	0.96	-11.63	1.02	<b>90.62</b> /9.38
	Single channel analysis			
	$\Lambda$	$E$	$r_{\text{RMS}}$	
	1.57	-0.31	4.94	
	1.79	-2.77	2.18	
	2.00	-6.69	1.53	
	$S$ - $D$ wave mixing analysis			
	$\Lambda$	$E$	$r_{\text{RMS}}$	$P(^4\mathbb{S}_{\frac{3}{2}}/^2\mathbb{D}_{\frac{3}{2}}/^4\mathbb{D}_{\frac{3}{2}})$
	1.47	-0.30	5.00	<b>99.22</b> /0.13/0.65
	1.74	-3.10	2.11	<b>98.82</b> /0.18/1.00
	2.00	-7.82	1.46	<b>99.05</b> /0.14/0.81
	Coupled channel analysis			
	$\Lambda$	$E$	$r_{\text{RMS}}$	$P(\Xi'_c D^*/\Xi_c^* D^*)$
	1.13	-1.04	2.90	<b>84.05</b> /5.95
	1.15	-6.12	1.17	<b>60.71</b> /39.29
	1.16	-10.09	0.91	<b>52.22</b> /47.28

When performing the single channel analysis with the cut-

off parameter over 0.92 GeV, the  $\Xi'_c D^*$  state with  $I(J^P) = 0(1/2^-)$  can form the loosely bound state. The bound state properties of the  $\Xi'_c D^*$  state with  $I(J^P) = 0(1/2^-)$  also can be discussed with the inclusion of the  $S$ - $D$  wave mixing effect, but the  $S$ - $D$  wave mixing effect does not have the significant impact on its bound state properties, as the contribution of the  $S$ -wave channel is over 99%. Furthermore, we can discuss the bound state properties of the  $\Xi'_c D^*$  state with  $I(J^P) = 0(1/2^-)$  by incorporating the coupled channel effect, which makes the cutoff parameter smaller when the same binding energy was achieved in the single channel analysis or the  $S$ - $D$  wave mixing analysis, of which the  $\Xi'_c D^*$  channel has the notable contribution of over 90 percent. Based on previous discussions, we propose the  $\Xi'_c D^*$  state with  $I(J^P) = 0(1/2^-)$  as the preferred candidate of the double-charm molecular pentaquark with single strangeness.

For the  $\Xi'_c D^*$  state with  $I(J^P) = 0(3/2^-)$ , when the cutoff parameter is 1.57 GeV in the single channel analysis, it has the loosely bound state solutions. After increasing the  $S$ - $D$  wave mixing effect, the loosely bound state solutions still exist with the cutoff parameter at 1.47 GeV, where the total contribution of the  $D$ -wave channels is less than 1 percent. Furthermore, when the contribution of the coupled channel effect by coupling the  $\Xi'_c D^*$  and  $\Xi_c^* D^*$  channels is further increased and the cutoff parameter is 1.13 GeV, the  $\Xi'_c D^*$  state with  $I(J^P) = 0(3/2^-)$  appears the loosely bound state solutions. At low binding energy, the  $\Xi'_c D^*$  channel dominates initially, but as the binding energy increases, the  $\Xi_c^* D^*$  channel also becomes a significant contribution. In conclusion, the  $\Xi'_c D^*$  state with  $I(J^P) = 0(3/2^-)$  can be recommended as the suitable candidate of the double-charm molecular pentaquark with single strangeness.

## 6. $\Xi_c^* D^*$ system

In Table VI, the bound state solutions for the  $\Xi_c^* D^*$  system are displayed. For the  $\Xi_c^* D^*$  states with  $I(J^P) = 1(1/2^-, 3/2^-)$ , the loosely bound state solutions are absent when the cutoff parameter is varied between 0.8 to 2.0 GeV and the  $S$ - $D$  wave mixing effect is taken into account. Thus, the  $\Xi_c^* D^*$  states with  $I(J^P) = 1(1/2^-, 3/2^-)$  are not supported as the candidates of the double-charm molecular pentaquarks with single strangeness.

In the following, we analyze the bound state properties for the  $\Xi_c^* D^*$  system, and find

- When conducting the single channel analysis with the cutoff parameter of 0.87 GeV, the  $\Xi_c^* D^*$  state with  $I(J^P) = 0(1/2^-)$  has the loosely bound state solutions. After increasing the mixing effect between the  $S$  and  $D$  waves, the cutoff parameter decreases to 0.85 MeV when the  $\Xi_c^* D^*$  state with  $I(J^P) = 0(1/2^-)$  appears the loosely bound state solutions, and the  $D$ -wave channel contribution is less than 1%. Thus, the  $\Xi_c^* D^*$  state with  $I(J^P) = 0(1/2^-)$  can be considered as the ideal candidate of the double-charm molecular pentaquark with single strangeness.



TABLE VI: The obtained bound state solutions for the  $\Xi_c^* D^*$  system. The units of the cutoff parameter  $\Lambda$ , binding energy  $E$ , and root-mean-square radius  $r_{\text{RMS}}$  are GeV, MeV, and fm, respectively. The primary probability of the corresponding channels is indicated in bold font.

Single channel analysis			$S$ - $D$ wave mixing analysis			
$I(J^P) = 0(\frac{1}{2}^-)$						
$\Lambda$	$E$	$r_{\text{RMS}}$	$\Lambda$	$E$	$r_{\text{RMS}}$	$P(^2\mathbb{S}_{\frac{1}{2}}/^4\mathbb{D}_{\frac{1}{2}}/^6\mathbb{D}_{\frac{1}{2}})$
0.87	-0.61	3.71	0.85	-0.43	4.24	<b>99.38</b> /0.37/0.25
0.91	-4.67	1.54	0.90	-4.71	1.57	<b>99.10</b> /0.55/0.35
0.95	-13.48	1.00	0.94	-12.70	1.04	<b>99.18</b> /0.51/0.31
$I(J^P) = 0(\frac{3}{2}^-)$						
$\Lambda$	$E$	$r_{\text{RMS}}$	$\Lambda$	$E$	$r_{\text{RMS}}$	$P(^4\mathbb{S}_{\frac{3}{2}}/^2\mathbb{D}_{\frac{3}{2}}/^4\mathbb{D}_{\frac{3}{2}}/^6\mathbb{D}_{\frac{3}{2}})$
1.03	-0.53	3.98	1.00	-0.31	4.74	<b>99.28</b> /0.20/0.47/0.06
1.08	-4.74	1.56	1.06	-4.34	1.66	<b>98.81</b> /0.33/0.77/0.09
1.13	-13.34	1.01	1.12	-13.70	1.02	<b>98.93</b> /0.30/0.69/0.08
$I(J^P) = 0(\frac{5}{2}^-)$						
$\Lambda$	$E$	$r_{\text{RMS}}$	$\Lambda$	$E$	$r_{\text{RMS}}$	$P(^6\mathbb{S}_{\frac{5}{2}}/^2\mathbb{D}_{\frac{5}{2}}/^4\mathbb{D}_{\frac{5}{2}}/^6\mathbb{D}_{\frac{5}{2}})$
1.65	-0.31	4.96	1.53	-0.32	4.95	<b>98.96</b> /0.07/0.07/0.95
1.83	-2.08	2.49	1.77	-2.50	2.34	<b>98.42</b> /0.09/0.05/1.44
2.00	-4.96	1.75	2.00	-6.31	1.63	<b>98.58</b> /0.08/0.04/1.30
$I(J^P) = 1(\frac{5}{2}^-)$						
			$\Lambda$	$E$	$r_{\text{RMS}}$	$P(^6\mathbb{S}_{\frac{5}{2}}/^2\mathbb{D}_{\frac{5}{2}}/^4\mathbb{D}_{\frac{5}{2}}/^6\mathbb{D}_{\frac{5}{2}})$
			1.74	-0.27	4.83	<b>99.48</b> /0.07/0.02/0.44
			1.87	-2.01	2.24	<b>98.85</b> /0.15/0.04/0.95
			2.00	-5.50	1.42	<b>98.32</b> /0.22/0.06/1.39

- When considering only the  $S$ -wave contribution and the cutoff parameter is greater than 1.03 GeV, the  $\Xi_c^* D^*$  state with  $I(J^P) = 0(3/2^-)$  can form the loosely bound state. Once the contribution of the  $D$ -wave channels is increased, the cutoff parameter for the  $\Xi_c^* D^*$  state with  $I(J^P) = 0(3/2^-)$  to form the loosely bound state decreases to 1.00 GeV, where the total contribution of the  $D$ -wave channels is less than 2 percent. In conclusion, the  $\Xi_c^* D^*$  state with  $I(J^P) = 0(3/2^-)$  can be regarded as the preferred candidate of the double-charm molecular pentaquark with single strangeness.
- In both the single channel analysis and the  $S$ - $D$  wave mixing analysis, the  $\Xi_c^* D^*$  state with  $I(J^P) = 0(5/2^-)$  starts to appear the loosely bound state solutions when the cutoff parameters are taken to be 1.65 GeV and 1.53 GeV, respectively. Here, the  $S$ -wave channel plays the major role and its contribution is greater than 98 percent. Consequently, we suggest that the  $\Xi_c^* D^*$  state with  $I(J^P) = 0(5/2^-)$  is the essential candidate of the double-charm molecular pentaquark with single strangeness.

- When conducting the single channel analysis with the cutoff parameter within the range of 0.8 to 2.0 GeV, the  $\Xi_c^* D^*$  state with  $I(J^P) = 1(5/2^-)$  is unable to form the loosely bound state. Considering the  $S$ - $D$  wave mixing analysis, the  $\Xi_c^* D^*$  state with  $I(J^P) = 1(5/2^-)$  can form the loosely bound state when the cutoff parameter is 1.74 GeV. Thus, the  $\Xi_c^* D^*$  state with  $I(J^P) = 1(5/2^-)$  can be considered as the possible candidate of the double-charm molecular pentaquark with single strangeness.

In our previous discussions, we have systematically investigated the bound state properties of the  $\Xi_c^{(*)} D^{(*)}$  systems by taking into account various effects, like the  $S$ - $D$  wave mixing effect and the coupled channel effect. Our findings indicate the existence of the ten most promising candidates of the double-charm molecular pentaquarks with single strangeness, including the  $\Xi_c D$  state with  $I(J^P) = 0(1/2^-)$ , the  $\Xi_c' D$  state with  $I(J^P) = 0(1/2^-)$ , the  $\Xi_c D^*$  states with  $I(J^P) = 0(1/2^-, 3/2^-)$ , the  $\Xi_c' D^*$  states with  $I(J^P) = 0(3/2^-)$ , the  $\Xi_c D^*$  states with  $I(J^P) = 0(1/2^-, 3/2^-)$ , and the  $\Xi_c' D^*$  states with  $I(J^P) = 0(1/2^-, 3/2^-, 5/2^-)$ , which is in agreement with the theoretical prediction presented in Ref. [128]. Furthermore, the  $\Xi_c^* D^*$  state with  $I(J^P) = 1(5/2^-)$  can be regarded as the possible candidate of the double-charm molecular pentaquark with single strangeness.

### III. THE M1 RADIATIVE DECAY BEHAVIORS AND THE MAGNETIC MOMENTS OF THE ISOSCALAR $\Xi_c^{(*)} D^{(*)}$ MOLECULAR PENTAQUARKS

By analyzing the mass spectra of the  $\Xi_c^{(*)} D^{(*)}$  molecular states, we have determined that the  $\Xi_c D$  state with  $I(J^P) = 0(1/2^-)$ , the  $\Xi_c' D$  state with  $I(J^P) = 0(1/2^-)$ , the  $\Xi_c D^*$  states with  $I(J^P) = 0(1/2^-, 3/2^-)$ , the  $\Xi_c' D^*$  state with  $I(J^P) = 0(3/2^-)$ , the  $\Xi_c D^*$  states with  $I(J^P) = 0(1/2^-, 3/2^-)$ , and the  $\Xi_c' D^*$  states with  $I(J^P) = 0(1/2^-, 3/2^-, 5/2^-)$  can be considered as the most promising candidates of the double-charm molecular pentaquarks with single strangeness, which can provide the important information for the experimental construction of the family of the  $\Xi_c^{(*)} D^{(*)}$ -type double-charm molecular pentaquarks with single strangeness. Nevertheless, the determination of their spin-parity quantum numbers is the important research topic if the relevant structures are observed within the corresponding energy regions in the future experiments. Furthermore, these molecular pentaquarks and the conventional  $\Omega_{cc}$  baryons [129] may share the same quantum number and similar mass. For instance, the  $\Xi_c' D$  state with  $I(J^P) = 0(1/2^-)$  and the  $\Omega_{cc}(1/2^-, 2P)$  state, the  $\Xi_c D^*$  state with  $I(J^P) = 0(3/2^-)$  and the  $\Omega_{cc}(3/2^-, 2P)$  state, the  $\Xi_c' D^*$  state with  $I(J^P) = 0(1/2^-)$  and the  $\Omega_{cc}(1/2^-, 3P)$  state, the  $\Xi_c D^*$  state with  $I(J^P) = 0(3/2^-)$  and the  $\Omega_{cc}(3/2^-, 3P)$  state, and so on [129]. Thus, the construction of the family of the  $\Xi_c^{(*)} D^{(*)}$ -type double-charm molecular pentaquarks with single strangeness will face the significant challenges in the future experiments. To identify the spin-parity quantum numbers and the configurations of the  $\Xi_c^{(*)} D^{(*)}$ -type double-charm

molecular pentaquarks with single strangeness experimentally, more physical observable need to be discussed based on the obtained mass spectra and spatial wave functions.

It is widely recognised that the electromagnetic properties of the hadron can indicate its inner structure, which is crucial for distinguishing the spin-parity quantum numbers and the configurations of the hadrons. This section concentrates on exploring the electromagnetic properties of our obtained isoscalar  $\Xi_c^{(*)}D^{(*)}$ -type double-charm molecular pentaquarks with single strangeness, and the constituent quark model is employed in our concrete calculations, which has been extensively employed in investigating the electromagnetic properties of the hadrons over the past years [52, 59–104].

### A. Formalism

In this work, we investigate the electromagnetic properties including the M1 radiative decay widths and the magnetic moments of our obtained isoscalar  $\Xi_c^{(*)}D^{(*)}$  molecular candidates. In the following, we focus on how to calculate the M1 radiative decay widths and the magnetic moments of our obtained isoscalar  $\Xi_c^{(*)}D^{(*)}$  molecular candidates based on the constituent quark model.

As shown in previous studies [52, 70, 76, 78, 83, 85–94, 99–102, 104, 130], the determination of the M1 radiative decay widths of the hadronic states can be achieved through analysis of the corresponding transition magnetic moments. For the  $H \rightarrow H'\gamma$  process, there exists the relation between the M1 radiative decay width, which is denoted as  $\Gamma_{H \rightarrow H'\gamma}$ , and the corresponding transition magnetic moment, which is marked as  $\mu_{H \rightarrow H'}$  [52, 94, 104], i.e.,

$$\Gamma_{H \rightarrow H'\gamma} = \frac{k^3}{m_p^2} \frac{\alpha_{\text{EM}}}{2J_H + 1} \frac{\sum_{J_{H'z}, J_{Hz}} \left( \begin{array}{ccc} J_{H'} & 1 & J_H \\ -J_{H'z} & 0 & J_{Hz} \end{array} \right)^2}{\left( \begin{array}{ccc} J_{H'} & 1 & J_H \\ -J_z & 0 & J_z \end{array} \right)^2} \frac{|\mu_{H \rightarrow H'}|^2}{\mu_N^2}. \quad (3.1)$$

Here, the emitted photon's momentum is represented by  $k$ , which can be calculated using the formula  $k = (m_H^2 - m_{H'}^2)/2m_H$ . The proton's mass is labelled as  $m_p$  and has a value of 938 MeV [125], and the electromagnetic fine structure constant, denoted by  $\alpha_{\text{EM}}$ , has an approximate value of 1/137. The lowest value between  $J_H$  and  $J_{H'}$  is designated as  $J_z$ , and we indicate the 3- $j$  coefficient through the notation

$$\left( \begin{array}{ccc} a & b & c \\ d & e & f \end{array} \right).$$

The isoscalar  $\Xi_c^{(*)}D^{(*)}$  molecular candidates have not yet been found experimentally [2–12]. However, their M1 radiative decay behaviors are dependent on their binding energies [52, 94, 104]. For simplicity, we adopt the same binding energies for the initial and final  $\Xi_c^{(*)}D^{(*)}$  molecular states to analyze their M1 radiative decay behaviors in this work. Based on

the aforementioned assumption, we can evaluate the transition magnetic moments between our obtained isoscalar  $\Xi_c^{(*)}D^{(*)}$  molecular candidates by calculating the following expectations [52, 70, 76, 78, 83, 85–94, 94, 99, 100, 104]

$$\mu_{H \rightarrow H'} = \left\langle J_{H'}, J_z \left| \sum_j \hat{\mu}_{zj}^{\text{spin}} e^{-i\mathbf{k} \cdot \mathbf{r}_j} + \hat{\mu}_z^{\text{orbital}} \right| J_H, J_z \right\rangle. \quad (3.2)$$

Here, we provide the definition of the  $z$ -component for both the spin magnetic moment operator and the orbital magnetic moment operator as follows [52, 59–104]

$$\hat{\mu}_{zj}^{\text{spin}} = \frac{e_j}{2m_j} \hat{\sigma}_{zj}, \quad (3.3)$$

$$\hat{\mu}_z^{\text{orbital}} = \left( \frac{m_m}{m_b + m_m} \frac{e_b}{2m_b} + \frac{m_b}{m_b + m_m} \frac{e_m}{2m_m} \right) \hat{L}_z, \quad (3.4)$$

where the electric charge, the mass, and the  $z$ -component of the Pauli spin operator of the  $j$ -th constituent of the hadron are indicated as  $e_j$ ,  $m_j$ , and  $\hat{\sigma}_{zj}$ , respectively. To differentiate between the baryons and the mesons within the hadronic molecular states, the subscripts  $b$  and  $m$  are used. Furthermore, the  $z$ -component of the orbital angular momentum operator between the meson and the baryon in the hadronic molecular state is denoted by  $\hat{L}_z$ .

Similarly, the magnetic moments of our obtained isoscalar  $\Xi_c^{(*)}D^{(*)}$  molecular candidates can be calculated using the following equation [52, 59–104]

$$\mu_H = \left\langle J_H, J_H \left| \sum_j \hat{\mu}_{zj}^{\text{spin}} + \hat{\mu}_z^{\text{orbital}} \right| J_H, J_H \right\rangle. \quad (3.5)$$

When studying the transition magnetic moments and the magnetic moments of the isoscalar  $\Xi_c^{(*)}D^{(*)}$  molecular candidates based on the constituent quark model, it is crucial to account for the spatial wave functions of both the molecular states and the corresponding constituent hadrons as the inputs [52, 94, 104]. For the isoscalar  $\Xi_c^{(*)}D^{(*)}$  molecular candidates, we utilize the precise spatial wave functions obtained by numerically solving the coupled channel Schrödinger equation in the previous section. For both the baryons  $\Xi_c^{(*)}$  and the mesons  $D^{(*)}$ , their spatial wave functions are described using the simple harmonic oscillator (SHO) wave function [52, 94, 104], i.e.,

$$\phi_{n,l,m}(\beta, \mathbf{r}) = \sqrt{\frac{2n!}{\Gamma(n+l+\frac{3}{2})}} L_n^{l+\frac{1}{2}}(\beta^2 r^2) \beta^{l+\frac{3}{2}} e^{-\frac{\beta^2 r^2}{2}} r^l Y_{lm}(\Omega_{\mathbf{r}}), \quad (3.6)$$

where the quantum numbers  $n$ ,  $l$ , and  $m$  are utilized to denote the radial, orbital, and magnetic characteristics of the hadron, respectively. To represent the associated Laguerre polynomial and the spherical harmonic function, we use the notations  $L_n^{l+\frac{1}{2}}(x)$  and  $Y_{lm}(\Omega_{\mathbf{r}})$ , respectively. The parameters in the SHO wave functions are denoted by  $\beta$ , which can be estimated by fitting their mass spectra [125]. In the specific calculations, we choose  $(\beta_p, \beta_\lambda)_{\Xi_c} = (0.301, 0.383)$ ,  $(\beta_p, \beta_\lambda)_{\Xi_c} =$

(0.252, 0.383),  $(\beta_p, \beta_\lambda)_{\Xi_c^*} = (0.243, 0.358)$ ,  $\beta_D = 0.357$ , and  $\beta_{D^*} = 0.307$  [131], which are expressed in the units of GeV. Furthermore, it is necessary to use the spherical Bessel function  $j_l(x)$  and the spherical harmonic function  $Y_{lm}(\Omega)$  to expand the spatial wave function of the emitted photon  $e^{-i\mathbf{k}\cdot\mathbf{r}_j}$  [132], i.e.,

$$e^{-i\mathbf{k}\cdot\mathbf{r}_j} = \sum_{l=0}^{\infty} \sum_{m=-l}^l 4\pi(-i)^l j_l(kr_j) Y_{lm}^*(\Omega_{\mathbf{k}}) Y_{lm}(\Omega_{\mathbf{r}_j}), \quad (3.7)$$

which can be used to calculate the contribution of the spatial wave functions of the initial and final states  $\langle \phi_f | e^{-i\mathbf{k}\cdot\mathbf{r}_j} | \phi_i \rangle$ .

### B. The transition magnetic moments and the magnetic moments of the baryons $\Xi_c^{(*)}$ and the mesons $D^{(*)}$

Within the constituent quark model, the transition magnetic moment of the hadronic molecular state can be expressed as the linear combination of the transition magnetic moments and the magnetic moments of the corresponding constituent hadrons [52, 94, 104]. Nevertheless, no experimental data is available on the associated transition magnetic moments and magnetic moments of the baryons  $\Xi_c^{(*)}$  and the mesons  $D^{(*)}$  at present [125]. Thus, we first discuss the transition magnetic moments and the magnetic moments of the baryons  $\Xi_c^{(*)}$  and the mesons  $D^{(*)}$  based on the constituent quark model. In this model, the quark masses serve as the essential input parameters, and the values of  $m_u = 0.336$  GeV,  $m_d = 0.336$  GeV,  $m_s = 0.450$  GeV, and  $m_c = 1.680$  GeV are utilized to conduct quantitative analyses of the hadronic transition magnetic moments and magnetic moments [52, 66, 91–94].

The flavour wave functions for the baryons  $\Xi_c^{(*)}$  and the mesons  $D^{(*)}$  can be constructed in the following manner

$$\begin{aligned} \Xi_c^+ &= \frac{1}{\sqrt{2}} (usc - suc), & \Xi_c^0 &= \frac{1}{\sqrt{2}} (dsc - sdc), \\ \Xi_c^{(*)+} &= \frac{1}{\sqrt{2}} (usc + suc), & \Xi_c^{(*)0} &= \frac{1}{\sqrt{2}} (dsc + sdc), \\ D^{(*)0} &= c\bar{u}, & D^{(*)+} &= c\bar{d}, \end{aligned}$$

and the spin wave functions  $|S, m_S\rangle$  corresponding to them can be constructed as

$$\begin{aligned} \Xi_c : & \begin{cases} \left| \frac{1}{2}, \frac{1}{2} \right\rangle = \frac{1}{\sqrt{2}} (\uparrow\downarrow\uparrow - \downarrow\uparrow\uparrow) \\ \left| \frac{1}{2}, -\frac{1}{2} \right\rangle = \frac{1}{\sqrt{2}} (\uparrow\downarrow\downarrow - \downarrow\uparrow\downarrow) \end{cases}, \\ \Xi_c' : & \begin{cases} \left| \frac{1}{2}, \frac{1}{2} \right\rangle = \frac{1}{\sqrt{6}} (2\uparrow\uparrow\downarrow - \downarrow\uparrow\uparrow - \uparrow\downarrow\uparrow) \\ \left| \frac{1}{2}, -\frac{1}{2} \right\rangle = \frac{1}{\sqrt{6}} (\uparrow\downarrow\uparrow + \uparrow\downarrow\downarrow - 2\downarrow\downarrow\uparrow) \end{cases}, \end{aligned}$$

$$\Xi_c^* : \begin{cases} \left| \frac{3}{2}, \frac{3}{2} \right\rangle = \uparrow\uparrow\uparrow \\ \left| \frac{3}{2}, \frac{1}{2} \right\rangle = \frac{1}{\sqrt{3}} (\downarrow\uparrow\uparrow + \uparrow\downarrow\uparrow + \uparrow\uparrow\downarrow) \\ \left| \frac{3}{2}, -\frac{1}{2} \right\rangle = \frac{1}{\sqrt{3}} (\downarrow\downarrow\uparrow + \uparrow\downarrow\downarrow + \downarrow\uparrow\downarrow) \\ \left| \frac{3}{2}, -\frac{3}{2} \right\rangle = \downarrow\downarrow\downarrow \end{cases},$$

$$D : |0, 0\rangle = \frac{1}{\sqrt{2}} (\uparrow\downarrow - \downarrow\uparrow),$$

$$D^* : \begin{cases} |1, 1\rangle = \uparrow\uparrow \\ |1, 0\rangle = \frac{1}{\sqrt{2}} (\uparrow\downarrow + \downarrow\uparrow) \\ |1, -1\rangle = \downarrow\downarrow \end{cases},$$

where the spins and the corresponding third components of these hadrons are denoted as the notations  $S$  and  $m_S$  in the spin wave functions  $|S, m_S\rangle$ , respectively. In addition, the third components of the spins of the quarks, which have values of  $+1/2$  and  $-1/2$ , are represented by the notations  $\uparrow$  and  $\downarrow$ , respectively.

Table VII presents our obtained results for the transition magnetic moments and the magnetic moments of the  $\Xi_c^{(*)}$  baryons and the  $D^{(*)}$  mesons, where we also compare our findings with those of the previous studies. When calculating the transition magnetic moments of the baryons  $\Xi_c^{(*)}$  and the mesons  $D^{(*)}$ , we take into account the contribution of the spatial wave functions for the initial and final states.

Based on the numerical results presented in Table VII, it is found that our obtained transition magnetic moments and magnetic moments for the baryons  $\Xi_c^{(*)}$  and the mesons  $D^{(*)}$  are consistent with those obtained from other works, which indicates that our adopted quark masses in the constituent quark model are dependable. Thus, our subsequent results can provide the important theoretical guidance for the future experimental investigations regarding the electromagnetic properties of the isoscalar  $\Xi_c^{(*)} D^{(*)}$  molecular candidates.

### C. The M1 radiative decay behaviors of the isoscalar $\Xi_c^{(*)} D^{(*)}$ molecular pentaquarks

Following the previous discussions, we now turn our attention to the electromagnetic properties including the M1 radiative decay behaviors and the magnetic moments of our obtained isoscalar  $\Xi_c^{(*)} D^{(*)}$  molecular candidates.

For the isoscalar  $\Xi_c^{(*)} D^{(*)}$  molecular states, the relevant flavour and spin-orbital wave functions have been constructed in the above section. Similar to the investigation of the mass spectra of the  $\Xi_c^{(*)} D^{(*)}$  molecular states, we also consider the influences of the  $S$ - $D$  wave mixing effect and the coupled channel effect in the study of their M1 radiative decay behaviors and magnetic moments. To derive the transition magnetic moments and the magnetic moments of the  $D$ -wave channels, their spin-orbital wave functions  $|^{2S+1}L_J\rangle$  need to be expanded

TABLE VII: Our obtained transition magnetic moments and magnetic moments of the baryons  $\Xi_c^{(*)}$  and the mesons  $D^{(*)}$ , and comparison with them obtained from other studies. The units for both the transition magnetic moments and the magnetic moments of the hadrons are  $\mu_N = e/2m_p$ .

Transition magnetic moments		
Decay processes	Our work	Other works
$\Xi_c'^+ \rightarrow \Xi_c^+ \gamma$	-1.412	-1.428 [89], -1.390 [66]
$\Xi_c'^0 \rightarrow \Xi_c^0 \gamma$	0.127	0.136 [93], 0.130 [66]
$\Xi_c^{*+} \rightarrow \Xi_c^+ \gamma$	1.904	1.940 [66], 1.960 [85]
$\Xi_c^{*0} \rightarrow \Xi_c^0 \gamma$	-0.163	-0.176 [87], -0.160 [133]
$\Xi_c^{*+} \rightarrow \Xi_c'^+ \gamma$	0.191	0.199 [94], 0.170 [66]
$\Xi_c^{*0} \rightarrow \Xi_c'^0 \gamma$	-1.106	-1.070 [85], -1.030 [85]
$D^{*0} \rightarrow D^0 \gamma$	2.140	2.134 [104], 2.233 [92]
$D^{*+} \rightarrow D^+ \gamma$	-0.525	-0.559 [92], -0.540 [134]
Magnetic moments		
Hadrons	Our work	Other works
$\Xi_c^+$	0.372	0.372 [93], 0.370 [66]
$\Xi_c^0$	0.372	0.372 [93], 0.366 [66]
$\Xi_c'^+$	0.654	0.654 [94], 0.650 [135]
$\Xi_c'^0$	-1.208	-1.208 [94], -1.200 [136]
$\Xi_c^{*+}$	1.539	1.539 [94], 1.510 [137]
$\Xi_c^{*0}$	-1.254	-1.254 [94], -1.260 [138]
$D^{*0}$	-1.489	-1.485 [104], -1.489 [92]
$D^{*+}$	1.303	1.308 [104], 1.303 [92]

through combining the spin wave function  $|S, m_S\rangle$  and the orbital wave function  $Y_{Lm_L}$ , i.e.,

$$|^{2S+1}L_J\rangle = \sum_{m_S, m_L} C_{S m_S, L m_L}^{J M} |S, m_S\rangle Y_{L m_L}. \quad (3.8)$$

As previously discussed, the transition magnetic moments and the M1 radiative decay behaviors of the hadronic molecular states depend on the bound energies of the initial and final hadronic molecular states [52, 94, 104]. However, these isoscalar  $\Xi_c^{(*)}D^{(*)}$  molecular candidates have yet to be discovered experimentally [2–12]. In this study, the same binding energies were utilised for both the initial and final  $\Xi_c^{(*)}D^{(*)}$  molecular states and three typical values -0.5, -6.0, and -12.0 MeV were taken to explore their transition magnetic moments and M1 radiative decay widths. In Tables VIII and IX, we summarise the transition magnetic moments and the M1 radiative decay widths of our obtained isoscalar  $\Xi_c^{(*)}D^{(*)}$  molecular candidates<sup>1</sup>.

For the isoscalar  $\Xi_c^{(*)}D^{(*)}$  molecular candidates, their M1 radiative decay behaviors are dependent on their transition magnetic moments and phase spaces [52, 92–94, 104], and this fact can be illustrated through the following two examples. Firstly, the  $\Xi_c^*D|3/2^-\rangle \rightarrow \Xi_c'D|1/2^-\rangle\gamma$  and the  $\Xi_c'D^*|3/2^-\rangle \rightarrow \Xi_c'D|1/2^-\rangle\gamma$  display similar transition magnetic moments, but the radiative decay width of the  $\Xi_c^*D|3/2^-\rangle \rightarrow \Xi_c'D|1/2^-\rangle\gamma$  is smaller than that of the  $\Xi_c'D^*|3/2^-\rangle \rightarrow \Xi_c'D|1/2^-\rangle\gamma$ , which is attributed to the fact that the phase space of the  $\Xi_c^*D|3/2^-\rangle \rightarrow \Xi_c'D|1/2^-\rangle\gamma$  is much smaller than that of the  $\Xi_c'D^*|3/2^-\rangle \rightarrow \Xi_c'D|1/2^-\rangle\gamma$ . Secondly, the  $\Xi_c^*D^*|1/2^-\rangle \rightarrow \Xi_c'D^*|3/2^-\rangle\gamma$  and the  $\Xi_c^*D^*|3/2^-\rangle \rightarrow \Xi_c'D^*|3/2^-\rangle\gamma$  have the same phase space. However, the M1 radiative decay width of the  $\Xi_c^*D^*|3/2^-\rangle \rightarrow \Xi_c'D^*|3/2^-\rangle\gamma$  is significantly larger than that of the  $\Xi_c^*D^*|1/2^-\rangle \rightarrow \Xi_c'D^*|3/2^-\rangle\gamma$ , which is due to the  $\Xi_c^*D^*|3/2^-\rangle \rightarrow \Xi_c'D^*|3/2^-\rangle\gamma$  has the stronger transition magnetic moment.

For the isoscalar  $\Xi_c^{(*)}D^{(*)}$  molecular candidates, their M1 radiative decay behaviors are dependent on the binding energies of the initial and final  $\Xi_c^{(*)}D^{(*)}$  molecular states [52, 94, 104], which is because the fact that the transition magnetic moments of the isoscalar  $\Xi_c^{(*)}D^{(*)}$  molecular candidates are influenced by the spatial wave functions of the initial and final  $\Xi_c^{(*)}D^{(*)}$  molecular states. In particular, the M1 radiative decay behaviors of our obtained isoscalar  $\Xi_c^{(*)}D^{(*)}$  molecular candidates are particularly affected by the changes in the binding energies of the corresponding initial and final  $\Xi_c^{(*)}D^{(*)}$  molecular states during the coupled channel analysis, this is mainly because there exists the significant change for the spatial wave functions of the different coupled channels as the binding energies change, which can be found in the previous section in the study of the mass spectra of the isoscalar  $\Xi_c^{(*)}D^{(*)}$  molecular candidates. Thus, the future experimental measurements of the binding energies of the isoscalar  $\Xi_c^{(*)}D^{(*)}$  molecular candidates can advance our comprehension of their M1 radiative decay behaviors.

In most cases, the  $S$ - $D$  wave mixing effect has the negligible effect on the M1 radiative decay widths of our obtained isoscalar  $\Xi_c^{(*)}D^{(*)}$  molecular candidates, and the coupled channel effect plays the crucial role in modifying the M1 radiative decay widths of our obtained isoscalar  $\Xi_c^{(*)}D^{(*)}$  molecular candidates, which exhibit the behavior similar to that of their mass spectra. As the binding energies of the initial and final  $\Xi_c^{(*)}D^{(*)}$  molecular states increase, the M1 radiative decay widths of the corresponding processes obtained through the coupled channel analysis diverge from those of the single channel analysis. This phenomenon can be attributed to the increasing contribution of other coupled channels as the binding energies of the initial and final  $\Xi_c^{(*)}D^{(*)}$  molecular states increase.

The study of the M1 radiative decay behaviors of the isoscalar  $\Xi_c^{(*)}D^{(*)}$  molecular candidates can provide the valu-

<sup>1</sup> In Tables VIII and IX, we labelled the radiative decay width less than

0.0005 keV as  $O(0)$ .



TABLE VIII: The transition magnetic moments  $\mu_{H \rightarrow H'}$  and the M1 radiative decay widths  $\Gamma_{H \rightarrow H' \gamma}$  of our obtained isoscalar  $\Xi_c^{(*)} D^{(*)}$  molecular candidates. Here, the results of the single channel analysis, the  $S$ - $D$  wave mixing analysis, and the coupled channel analysis are represented by Cases I, II, and III in the second column, respectively.

Radiative decay processes	Cases	$\mu_{H \rightarrow H'} (\mu_N)$	$\Gamma_{H \rightarrow H' \gamma} (\text{keV})$
$\Xi_c' D \left  \frac{1}{2}^- \right\rangle \rightarrow \Xi_c D \left  \frac{1}{2}^- \right\rangle \gamma$	I	-0.550, -0.629, -0.635	3.168, 4.135, 4.212
	III	-0.417, -0.202, -0.015	1.817, 0.425, 0.002
$\Xi_c D^* \left  \frac{3}{2}^- \right\rangle \rightarrow \Xi_c D \left  \frac{1}{2}^- \right\rangle \gamma$	I	0.467, 0.624, 0.639	2.434, 4.349, 4.562
	III	0.316, 0.199, 0.110	1.113, 0.441, 0.134
$\Xi_c D^* \left  \frac{1}{2}^- \right\rangle \rightarrow \Xi_c D \left  \frac{1}{2}^- \right\rangle \gamma$	I	0.330, 0.441, 0.452	2.434, 4.349, 4.562
	III	0.314, 0.379, 0.385	2.206, 3.197, 3.305
$\Xi_c^* D \left  \frac{3}{2}^- \right\rangle \rightarrow \Xi_c D \left  \frac{1}{2}^- \right\rangle \gamma$	I	0.620, 0.824, 0.843	8.272, 14.592, 15.275
	III	0.591, 0.525, 0.281	7.503, 5.919, 1.698
$\Xi_c' D^* \left  \frac{1}{2}^- \right\rangle \rightarrow \Xi_c D \left  \frac{1}{2}^- \right\rangle \gamma$	III	0.024, 0.101, 0.153	0.069, 1.227, 2.828
$\Xi_c' D^* \left  \frac{3}{2}^- \right\rangle \rightarrow \Xi_c D \left  \frac{1}{2}^- \right\rangle \gamma$	III	-0.008, -0.031, -0.040	0.004, 0.058, 0.094
$\Xi_c^* D^* \left  \frac{1}{2}^- \right\rangle \rightarrow \Xi_c D \left  \frac{1}{2}^- \right\rangle \gamma$	III	0.013, 0.017, 0.029	0.038, 0.070, 0.201
$\Xi_c^* D^* \left  \frac{3}{2}^- \right\rangle \rightarrow \Xi_c D \left  \frac{1}{2}^- \right\rangle \gamma$	III	-0.003, -0.012, -0.056	0.001, 0.016, 0.373
$\Xi_c D^* \left  \frac{3}{2}^- \right\rangle \rightarrow \Xi_c' D \left  \frac{1}{2}^- \right\rangle \gamma$	III	-0.068, -0.104, -0.088	0.001, 0.001, 0.001
$\Xi_c D^* \left  \frac{1}{2}^- \right\rangle \rightarrow \Xi_c' D \left  \frac{1}{2}^- \right\rangle \gamma$	III	0.057, 0.179, 0.230	0.001, 0.008, 0.014
$\Xi_c^* D \left  \frac{3}{2}^- \right\rangle \rightarrow \Xi_c' D \left  \frac{1}{2}^- \right\rangle \gamma$	I	-0.429, -0.453, -0.455	0.227, 0.253, 0.255
	III	-0.368, -0.151, -0.017	0.167, 0.028, $\phi(0)$
$\Xi_c' D^* \left  \frac{1}{2}^- \right\rangle \rightarrow \Xi_c' D \left  \frac{1}{2}^- \right\rangle \gamma$	I	0.336, 0.442, 0.452	2.523, 4.371, 4.567
	III	0.336, 0.365, 0.319	2.522, 2.976, 2.274
$\Xi_c' D^* \left  \frac{3}{2}^- \right\rangle \rightarrow \Xi_c' D \left  \frac{1}{2}^- \right\rangle \gamma$	I	0.462, 0.610, 0.627	2.380, 4.161, 4.391
	III	0.333, 0.252, 0.196	1.239, 0.707, 0.428
$\Xi_c^* D^* \left  \frac{1}{2}^- \right\rangle \rightarrow \Xi_c' D \left  \frac{1}{2}^- \right\rangle \gamma$	III	-0.089, -0.201, -0.230	0.557, 2.839, 3.722
$\Xi_c^* D^* \left  \frac{3}{2}^- \right\rangle \rightarrow \Xi_c' D \left  \frac{1}{2}^- \right\rangle \gamma$	III	0.088, 0.196, 0.220	0.273, 1.344, 1.703
$\Xi_c^* D \left  \frac{3}{2}^- \right\rangle \rightarrow \Xi_c D^* \left  \frac{3}{2}^- \right\rangle \gamma$	III	0.115, 0.573, 0.787	0.003, 0.066, 0.123
$\Xi_c' D^* \left  \frac{1}{2}^- \right\rangle \rightarrow \Xi_c D^* \left  \frac{3}{2}^- \right\rangle \gamma$	I	-0.523, -0.592, -0.597	2.858, 3.670, 3.730
	III	-0.479, -0.438, -0.389	2.401, 2.006, 1.585
$\Xi_c' D^* \left  \frac{3}{2}^- \right\rangle \rightarrow \Xi_c D^* \left  \frac{3}{2}^- \right\rangle \gamma$	I	-0.548, -0.619, -0.625	1.744, 2.225, 2.269
	III	-0.645, -0.865, -0.904	2.421, 4.350, 4.753
$\Xi_c^* D^* \left  \frac{1}{2}^- \right\rangle \rightarrow \Xi_c D^* \left  \frac{3}{2}^- \right\rangle \gamma$	I	-0.149, -0.194, -0.199	0.959, 1.628, 1.698
	III	-0.089, -0.055, -0.043	0.344, 0.131, 0.078
$\Xi_c^* D^* \left  \frac{3}{2}^- \right\rangle \rightarrow \Xi_c D^* \left  \frac{3}{2}^- \right\rangle \gamma$	I	-0.400, -0.521, -0.533	6.886, 11.718, 12.226
	III	-0.491, -0.702, -0.735	10.376, 21.265, 23.296
$\Xi_c^* D^* \left  \frac{5}{2}^- \right\rangle \rightarrow \Xi_c D^* \left  \frac{3}{2}^- \right\rangle \gamma$	I	0.472, 0.623, 0.634	7.988, 13.955, 14.435
	III	0.395, 0.398, 0.360	5.604, 5.677, 4.659

able information to reflect their inner structures and properties, which may offer the vital insights for the future experimental determination of their spin-parity quantum numbers. A notable dissimilarity is observed in the M1 radiative decay behaviors of the  $\Xi_c D^* \left| 1/2^- \right\rangle \rightarrow \Xi_c D^* \left| 3/2^- \right\rangle \gamma$  and the

$\Xi_c^* D^* \left| 3/2^- \right\rangle \rightarrow \Xi_c D^* \left| 3/2^- \right\rangle \gamma$ , so this allows for the future experimental differentiation of the  $\Xi_c D^*$  molecular state with  $I(J^P) = 0(1/2^-)$  and the  $\Xi_c^* D^*$  molecular state with  $I(J^P) = 0(3/2^-)$  through the analysis of their M1 radiative decay behaviors. Many similar examples exist in the present work,

TABLE IX: The transition magnetic moments  $\mu_{H \rightarrow H' \gamma}$  and the M1 radiative decay widths  $\Gamma_{H \rightarrow H' \gamma}$  of our obtained isoscalar  $\Xi_c^{(*)} D^{(*)}$  molecular candidates. Here, the results of the single channel analysis, the  $S$ - $D$  wave mixing analysis, and the coupled channel analysis are represented by Cases I, II, and III in the second column, respectively.

Radiative decay processes	Cases	$\mu_{H \rightarrow H' \gamma} (\mu_N)$	$\Gamma_{H \rightarrow H' \gamma} (\text{keV})$
$\Xi_c^* D \left  \frac{3}{2}^- \right\rangle \rightarrow \Xi_c D^* \left  \frac{1}{2}^- \right\rangle \gamma$	III	0.037, 0.060, 0.028	$o(0)$ , 0.001, $o(0)$
$\Xi_c' D^* \left  \frac{1}{2}^- \right\rangle \rightarrow \Xi_c D^* \left  \frac{1}{2}^- \right\rangle \gamma$	I	0.185, 0.209, 0.211	0.357, 0.459, 0.466
	III	0.148, 0.084, 0.042	0.228, 0.075, 0.019
$\Xi_c' D^* \left  \frac{3}{2}^- \right\rangle \rightarrow \Xi_c D^* \left  \frac{1}{2}^- \right\rangle \gamma$	I	-0.516, -0.583, -0.589	1.395, 1.780, 1.815
	III	-0.423, -0.273, -0.206	0.937, 0.391, 0.222
$\Xi_c^* D^* \left  \frac{1}{2}^- \right\rangle \rightarrow \Xi_c D^* \left  \frac{1}{2}^- \right\rangle \gamma$	I	-0.422, -0.550, -0.561	7.674, 13.025, 13.584
	III	-0.392, -0.434, -0.403	6.620, 8.126, 7.002
$\Xi_c^* D^* \left  \frac{3}{2}^- \right\rangle \rightarrow \Xi_c D^* \left  \frac{1}{2}^- \right\rangle \gamma$	I	0.471, 0.614, 0.628	4.782, 8.137, 8.490
	III	0.428, 0.457, 0.414	3.956, 4.500, 3.684
$\Xi_c' D^* \left  \frac{1}{2}^- \right\rangle \rightarrow \Xi_c^* D \left  \frac{3}{2}^- \right\rangle \gamma$	III	-0.044, -0.214, -0.280	0.006, 0.151, 0.259
$\Xi_c' D^* \left  \frac{3}{2}^- \right\rangle \rightarrow \Xi_c^* D \left  \frac{3}{2}^- \right\rangle \gamma$	III	0.110, 0.335, 0.349	0.022, 0.206, 0.223
$\Xi_c^* D^* \left  \frac{1}{2}^- \right\rangle \rightarrow \Xi_c^* D \left  \frac{3}{2}^- \right\rangle \gamma$	I	-0.337, -0.443, -0.452	2.539, 4.381, 4.573
	III	-0.325, -0.277, -0.132	2.359, 1.717, 0.388
$\Xi_c^* D^* \left  \frac{3}{2}^- \right\rangle \rightarrow \Xi_c^* D \left  \frac{3}{2}^- \right\rangle \gamma$	I	0.451, 0.594, 0.607	2.531, 4.378, 4.572
	III	0.455, 0.556, 0.467	2.571, 3.839, 2.712
$\Xi_c^* D^* \left  \frac{5}{2}^- \right\rangle \rightarrow \Xi_c^* D \left  \frac{3}{2}^- \right\rangle \gamma$	I	0.354, 0.472, 0.480	2.339, 4.145, 4.290
	III	0.356, 0.367, 0.240	2.365, 2.513, 1.076
$\Xi_c^* D^* \left  \frac{1}{2}^- \right\rangle \rightarrow \Xi_c' D^* \left  \frac{1}{2}^- \right\rangle \gamma$	I	0.288, 0.303, 0.303	0.204, 0.225, 0.227
	II	0.287, 0.302, 0.303	0.203, 0.225, 0.226
	III	0.293, 0.316, 0.319	0.211, 0.245, 0.250
$\Xi_c^* D^* \left  \frac{3}{2}^- \right\rangle \rightarrow \Xi_c' D^* \left  \frac{1}{2}^- \right\rangle \gamma$	I	-0.322, -0.338, -0.339	0.128, 0.141, 0.142
	II	-0.320, -0.336, -0.338	0.126, 0.139, 0.140
	III	-0.313, -0.302, -0.284	0.120, 0.113, 0.100
$\Xi_c^* D^* \left  \frac{1}{2}^- \right\rangle \rightarrow \Xi_c' D^* \left  \frac{3}{2}^- \right\rangle \gamma$	I	0.100, 0.104, 0.104	0.025, 0.026, 0.027
	II	0.100, 0.105, 0.104	0.025, 0.027, 0.027
	III	0.119, 0.154, 0.163	0.035, 0.059, 0.065
$\Xi_c^* D^* \left  \frac{3}{2}^- \right\rangle \rightarrow \Xi_c' D^* \left  \frac{3}{2}^- \right\rangle \gamma$	I	0.270, 0.279, 0.279	0.100, 0.106, 0.106
	II	0.270, 0.281, 0.279	0.100, 0.108, 0.107
	III	0.268, 0.258, 0.244	0.098, 0.091, 0.082
$\Xi_c^* D^* \left  \frac{5}{2}^- \right\rangle \rightarrow \Xi_c' D^* \left  \frac{3}{2}^- \right\rangle \gamma$	I	-0.331, -0.350, -0.352	0.225, 0.251, 0.254
	II	-0.330, -0.349, -0.351	0.223, 0.250, 0.252
	III	-0.295, -0.209, -0.167	0.179, 0.090, 0.057

like the  $\Xi_c' D^* |1/2^- \rangle \rightarrow \Xi_c D^* |1/2^- \rangle \gamma$  and the  $\Xi_c' D^* |3/2^- \rangle \rightarrow \Xi_c D^* |1/2^- \rangle \gamma$ , the  $\Xi_c^* D^* |1/2^- \rangle \rightarrow \Xi_c' D^* |1/2^- \rangle \gamma$  and the  $\Xi_c^* D^* |1/2^- \rangle \rightarrow \Xi_c' D^* |3/2^- \rangle \gamma$ , and so on.

Similarly to the M1 radiative decay behaviors of the  $\Xi_c \bar{D}^* |3/2^- \rangle \rightarrow \Xi_c \bar{D} |1/2^- \rangle \gamma$  and  $\Xi_c \bar{D}^* |1/2^- \rangle \rightarrow \Xi_c \bar{D} |1/2^- \rangle \gamma$  processes [93], the same M1 radiative decay behaviors are found in the  $\Xi_c D^* |3/2^- \rangle \rightarrow \Xi_c D |1/2^- \rangle \gamma$  and

$\Xi_c D^* |1/2^- \rangle \rightarrow \Xi_c D |1/2^- \rangle \gamma$  processes when limited to the single channel analysis, which can be attributed to the same binding properties for the  $\Xi_c D^*$  molecular state with  $I(J^P) = 0(1/2^-)$  and the  $\Xi_c D^*$  molecular state with  $I(J^P) = 0(3/2^-)$  in the single channel analysis. Thus, it is challenging to distinguish the  $\Xi_c D^*$  molecular state with  $I(J^P) = 0(1/2^-)$  and the  $\Xi_c D^*$  molecular state with  $I(J^P) = 0(3/2^-)$  based on the study

of the M1 radiative decay behaviors for the  $\Xi_c D^* |3/2^- \rangle \rightarrow \Xi_c D |1/2^- \rangle \gamma$  and  $\Xi_c D^* |1/2^- \rangle \rightarrow \Xi_c D |1/2^- \rangle \gamma$  processes in the single channel analysis. However, the M1 radiative decay behaviors of the  $\Xi_c D^* |3/2^- \rangle \rightarrow \Xi_c D |1/2^- \rangle \gamma$  and  $\Xi_c D^* |1/2^- \rangle \rightarrow \Xi_c D |1/2^- \rangle \gamma$  processes exhibit the difference by introducing the coupled channel effect. Consequently, this finding indicates that the  $\Xi_c D^*$  molecular state with  $I(J^P) = 0(1/2^-)$  and the  $\Xi_c D^*$  molecular state with  $I(J^P) = 0(3/2^-)$  can be distinguished based on the study of the M1 radiative decay behaviors for the  $\Xi_c D^* |3/2^- \rangle \rightarrow \Xi_c D |1/2^- \rangle \gamma$  and  $\Xi_c D^* |1/2^- \rangle \rightarrow \Xi_c D |1/2^- \rangle \gamma$  processes after accounting for the influence of the coupled channel effect.

When considering the same binding energies for the initial and final  $\Xi_c^{(*)} D^{(*)}$  molecular states, the radiative decay widths involving the same system with different spin-parity quantum numbers for the initial and final states are zero, and this occurs as a result of the phase spaces for such processes being zero [92, 93, 104]. In fact, there may be differences for the binding energies of the initial and final  $\Xi_c^{(*)} D^{(*)}$  molecular states for such M1 radiative decay processes. However, their M1 radiative decay widths are strongly suppressed (refer to Table X for more information), which is due to the limited phase spaces for such M1 radiative decay processes.

TABLE X: The transition magnetic moments and the M1 radiative decay widths of our obtained isoscalar  $\Xi_c^{(*)} D^{(*)}$  molecular candidates, which involve the same system with different spin-parity quantum numbers for the initial and final states. The transition magnetic moments are expressed in  $\mu_N$  units, and the radiative decay widths are measured in keV. Here, the results of the single channel analysis, the  $S$ - $D$  wave mixing analysis, and the coupled channel analysis are represented by Cases I, II, and III in the second column, respectively.  $\Gamma_{H \rightarrow H' \gamma}^{\text{Max}}$  indicates the maximum value of the M1 radiative decay width when varying the binding energies of the corresponding initial and final molecular states.

Decay processes	Cases	$\mu_{H \rightarrow H'}$	$\Gamma_{H \rightarrow H' \gamma}^{\text{Max}}$
$\Xi_c D^*  1/2^- \rangle \rightarrow \Xi_c D^*  3/2^- \rangle \gamma$	I	0.395, 0.395, 0.395	0.002
	III	0.306, 0.139, 0.077	
$\Xi_c' D^*  3/2^- \rangle \rightarrow \Xi_c' D^*  1/2^- \rangle \gamma$	I	-0.215, -0.211, -0.210	0.0006
	II	-0.214, -0.211, -0.209	
$\Xi_c D^*  3/2^- \rangle \rightarrow \Xi_c D^*  1/2^- \rangle \gamma$	I	0.140, 0.140, 0.140	0.0001
	II	0.139, 0.139, 0.139	
$\Xi_c D^*  5/2^- \rangle \rightarrow \Xi_c D^*  3/2^- \rangle \gamma$	I	0.091, 0.089, 0.088	0.00009
	II	0.090, 0.088, 0.087	

#### D. The magnetic moments of the isoscalar $\Xi_c^{(*)} D^{(*)}$ molecular pentaquarks

In Table XI, we list the magnetic moments of our obtained isoscalar  $\Xi_c^{(*)} D^{(*)}$  molecular candidates. In the specific calculations, the relevant numerical results were obtained through

the single channel analysis, the  $S$ - $D$  wave mixing analysis, and the coupled channel analysis, respectively. For the  $S$ - $D$  wave mixing analysis and the coupled channel analysis, we take the binding energies  $-0.5$ ,  $-6.0$ , and  $-12.0$  MeV for the isoscalar  $\Xi_c^{(*)} D^{(*)}$  molecular candidates to discuss their magnetic moments.

TABLE XI: The magnetic moments of our obtained isoscalar  $\Xi_c^{(*)} D^{(*)}$  molecular candidates. The units of the magnetic moments of the hadrons are  $\mu_N$ . Here, the results of the single channel analysis, the  $S$ - $D$  wave mixing analysis, and the coupled channel analysis are represented by Cases I, II, and III, respectively.

Hadrons	Case I	Case II	Case III
$\Xi_c D  1/2^- \rangle$	0.372		0.371, 0.368, 0.370
$\Xi_c' D  1/2^- \rangle$	-0.277		-0.151, 0.061, 0.147
$\Xi_c D^*  3/2^- \rangle$	0.279		0.403, 0.638, 0.745
$\Xi_c D^*  1/2^- \rangle$	-0.186		-0.111, 0.043, 0.100
$\Xi_c' D^*  3/2^- \rangle$	0.143		0.213, 0.527, 0.560
$\Xi_c' D^*  1/2^- \rangle$	0.030	0.031, 0.032, 0.032	0.065, 0.148, 0.198
$\Xi_c' D^*  3/2^- \rangle$	-0.370	-0.364, -0.363, -0.365	-0.245, 0.026, 0.102
$\Xi_c D^*  1/2^- \rangle$	0.110	0.111, 0.111, 0.111	
$\Xi_c D^*  3/2^- \rangle$	0.067	0.070, 0.071, 0.070	
$\Xi_c D^*  5/2^- \rangle$	0.050	0.052, 0.053, 0.052	

Based on the numerical results listed in Table XI, we find that

- In most cases, the  $S$ - $D$  wave mixing effect has the negligible impact on the magnetic moments of our obtained isoscalar  $\Xi_c^{(*)} D^{(*)}$  molecular candidates, and the coupled channel effect plays the crucial role in modifying the magnetic moments of our obtained isoscalar  $\Xi_c^{(*)} D^{(*)}$  molecular candidates.
- In the coupled channel analysis, it is evident that the magnetic moments of our obtained isoscalar  $\Xi_c^{(*)} D^{(*)}$  molecular candidates depend on the corresponding binding energies. Therefore, we strongly recommend the experimental determination of the binding energies of our obtained isoscalar  $\Xi_c^{(*)} D^{(*)}$  molecular candidates, which is crucial for enhancing the understanding of the magnetic moments of our obtained isoscalar  $\Xi_c^{(*)} D^{(*)}$  molecular candidates.
- The magnetic moments of our obtained isoscalar  $\Xi_c^{(*)} D^{(*)}$  molecular candidates can reflect their inner structures and properties, and the determination of the spin-parity quantum numbers of these molecular pentaquarks can be achieved experimentally through the study of their magnetic moments in the future, such as the  $\Xi_c D^*$  state with  $I(J^P) = 0(1/2^-)$  and the  $\Xi_c D^*$  state with  $I(J^P) = 0(3/2^-)$ , the  $\Xi_c' D^*$  state with  $I(J^P) = 0(1/2^-)$  and the  $\Xi_c' D^*$  state with  $I(J^P) = 0(3/2^-)$ , and so on.

#### IV. SUMMARY

In the field of the hadron physics, the search for the exotic hadronic matter presents the compelling and vital area of research. Through the accumulation of the experimental data, LHCb has detected the candidates of the hidden-charm pentaquarks with strangeness  $P_{\psi_s}^\Lambda(4459)/P_{\psi_s}^\Lambda(4338)$  and the double-charm tetraquark state  $T_{cc}(3875)^+$ , which has led the researchers to believe that the family of the double-charm molecular pentaquarks may exist within the hadron spectroscopy. Within the OBE model through the incorporation of both the  $S$ - $D$  wave mixing effect and the coupled channel effect, the existence of the double-charm molecular pentaquark candidates including the  $\Sigma_c^{(*)}D^{(*)}$ ,  $\Xi_c^{(\prime,*)}D^{(*)}$ , and  $\Omega_c^{(*)}D_s^{(*)}$  types have been predicted [50–52]. In the present work, the  $\Xi_c^{(\prime,*)}D^{(*)}$  molecular systems are the main research objects.

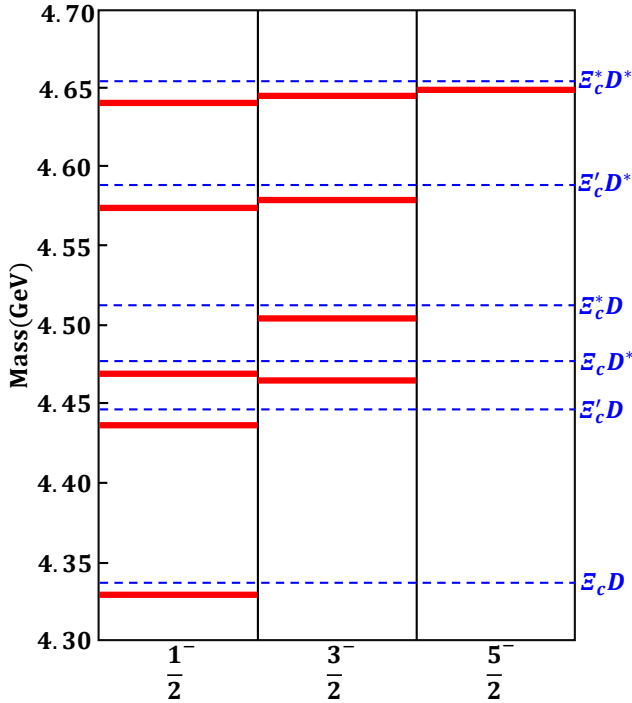


FIG. 3: Our established mass spectra of the isoscalar  $\Xi_c^{(\prime,*)}D^{(*)}$ -type double-charm molecular pentaquark candidates with single strangeness. Here, the thresholds of the corresponding  $\Xi_c^{(\prime,*)}D^{(*)}$  channels are plotted with the blue dotted lines, and the most promising candidates of the isoscalar  $\Xi_c^{(\prime,*)}D^{(*)}$ -type double-charm molecular pentaquarks with single strangeness are depicted with the red thick solid lines.

Firstly, we obtain the mass spectra and the corresponding spatial wave functions of the  $\Xi_c^{(\prime,*)}D^{(*)}$ -type double-charm molecular pentaquark candidates with single strangeness. Our calculations investigate the interactions between the  $\Xi_c^{(\prime,*)}D^{(*)}$  systems by utilizing the OBE model and considering both the  $S$ - $D$  wave mixing effect and the coupled channel effect, and their bound state properties can then be analyzed by solving

the coupled channel Schrödinger equation. Our investigations has revealed the existence of the ten most promising candidates of the double-charm molecular pentaquarks with single strangeness, including the  $\Xi_c D$  state with  $I(J^P) = 0(1/2^-)$ , the  $\Xi_c' D$  state with  $I(J^P) = 0(1/2^-)$ , the  $\Xi_c D^*$  states with  $I(J^P) = 0(1/2^-, 3/2^-)$ , the  $\Xi_c^* D$  state with  $I(J^P) = 0(3/2^-)$ , the  $\Xi_c' D^*$  states with  $I(J^P) = 0(1/2^-, 3/2^-)$ , and the  $\Xi_c^* D^*$  states with  $I(J^P) = 0(1/2^-, 3/2^-, 5/2^-)$  (see Fig. 3 for more details), which is in accordance with the theoretical analysis presented in Ref. [128]. Moreover, the  $\Xi_c D^*$  molecules with  $I(J^P) = 0(1/2^-, 3/2^-)$  and the  $\Xi_c \bar{D}^*$  molecules with  $I(J^P) = 0(1/2^-, 3/2^-)$  [36] display similar spectral behavior, and the  $\Xi_c D^*$  molecular states with  $I(J^P) = 0(1/2^-, 3/2^-)$  can be separated into two states owing to the contribution of the coupled channel effect.

After that, we evaluate the M1 radiative decay behaviors and the magnetic moments of the isoscalar  $\Xi_c^{(\prime,*)}D^{(*)}$  molecular states based on the obtained mass spectra and spatial wave functions. Our calculations employ the constituent quark model and account for both the  $S$ - $D$  wave mixing effect and the coupled channel effect. Based on our numerical calculations, we find that the study of the M1 radiative decay behaviors of the isoscalar  $\Xi_c^{(\prime,*)}D^{(*)}$  molecules can yield the significant insights for the future experiments to determine their spin-parity quantum numbers, and the M1 radiative decay behaviors of the  $\Xi_c D^* |3/2^- \rangle \rightarrow \Xi_c D |1/2^- \rangle \gamma$  and  $\Xi_c D^* |1/2^- \rangle \rightarrow \Xi_c D |1/2^- \rangle \gamma$  processes are similar to those of the  $\Xi_c \bar{D}^* |3/2^- \rangle \rightarrow \Xi_c \bar{D} |1/2^- \rangle \gamma$  and  $\Xi_c \bar{D}^* |1/2^- \rangle \rightarrow \Xi_c \bar{D} |1/2^- \rangle \gamma$  processes [93]. Furthermore, the magnetic moments of the isoscalar  $\Xi_c^{(\prime,*)}D^{(*)}$  molecular candidates can provide the valuable information to reflect their inner structures and properties.

With the accumulation of the increased statistical data during the LHCb's Run II and Run III status [139], there is a good chance that LHCb can detect the double-charm molecular pentaquarks. We strongly recommend that the future experimental research should focus on the isoscalar  $\Xi_c^{(\prime,*)}D^{(*)}$  molecular pentaquarks, which not only enrich the family of the double-charm molecular states, but also test the interpretation of the observed  $P_{\psi_s}^\Lambda(4459)$ ,  $P_{\psi_s}^\Lambda(4338)$ , and  $T_{cc}(3875)^+$  states as the  $\Xi_c \bar{D}^*$ ,  $\Xi_c \bar{D}$ , and  $DD^*$  molecular states.

#### ACKNOWLEDGMENTS

This work is supported by the China National Funds for Distinguished Young Scientists under Grant No. 11825503, National Key Research and Development Program of China under Contract No. 2020YFA0406400, the 111 Project under Grant No. B20063, the fundamental Research Funds for the Central Universities, the project for top-notch innovative talents of Gansu province, and the National Natural Science Foundation of China under Grant Nos. 12335001, 12247155 and 12247101. F.L.W. is also supported by the China Postdoctoral Science Foundation under Grant No. 2022M721440.



- 
- [1] S. K. Choi *et al.* (Belle Collaboration), Observation of a Narrow Charmonium-Like State in Exclusive  $B^\pm \rightarrow K^\pm \pi^\mp J/\psi$  Decays, *Phys. Rev. Lett.* **91**, 262001 (2003).
- [2] X. Liu, An overview of XYZ new particles, *Chin. Sci. Bull.* **59**, 3815 (2014).
- [3] A. Hosaka, T. Iijima, K. Miyabayashi, Y. Sakai, and S. Yasui, Exotic hadrons with heavy flavors:  $X$ ,  $Y$ ,  $Z$ , and related states, *Prog. Theor. Exp. Phys.* **2016**, 062C01 (2016).
- [4] H. X. Chen, W. Chen, X. Liu, and S. L. Zhu, The hidden-charm pentaquark and tetraquark states, *Phys. Rep.* **639**, 1 (2016).
- [5] J. M. Richard, Exotic hadrons: review and perspectives, *Few Body Syst.* **57**, 1185-1212 (2016).
- [6] R. F. Lebed, R. E. Mitchell and E. S. Swanson, Heavy-Quark QCD Exotica, *Prog. Part. Nucl. Phys.* **93**, 143-194 (2017).
- [7] S. L. Olsen, T. Skwarnicki, and D. Zieminska, Nonstandard heavy mesons and baryons: Experimental evidence, *Rev. Mod. Phys.* **90**, 015003 (2018).
- [8] F. K. Guo, C. Hanhart, U. G. Meißner, Q. Wang, Q. Zhao, and B. S. Zou, Hadronic molecules, *Rev. Mod. Phys.* **90**, 015004 (2018).
- [9] Y. R. Liu, H. X. Chen, W. Chen, X. Liu, and S. L. Zhu, Pentaquark and tetraquark states, *Prog. Part. Nucl. Phys.* **107**, 237 (2019).
- [10] N. Brambilla, S. Eidelman, C. Hanhart, A. Nefediev, C. P. Shen, C. E. Thomas, A. Vairo, and C. Z. Yuan, The XYZ states: Experimental and theoretical status and perspectives, *Phys. Rep.* **873**, 1 (2020).
- [11] L. Meng, B. Wang, G. J. Wang and S. L. Zhu, Chiral perturbation theory for heavy hadrons and chiral effective field theory for heavy hadronic molecules, *Phys. Rept.* **1019**, 1-149 (2023).
- [12] H. X. Chen, W. Chen, X. Liu, Y. R. Liu and S. L. Zhu, An updated review of the new hadron states, *Rept. Prog. Phys.* **86**, no.2, 026201 (2023).
- [13] M. Gell-Mann, A Schematic Model of Baryons and Mesons, *Phys. Lett.* **8**, 214 (1964).
- [14] G. Zweig, An SU(3) model for strong interaction symmetry and its breaking. Version 1, *CERN-TH.401*.
- [15] R. Aaij *et al.* (LHCb Collaboration), Observation of a narrow pentaquark state,  $P_c(4312)^+$ , and of two-peak structure of the  $P_c(4450)^+$ , *Phys. Rev. Lett.* **122**, 222001 (2019).
- [16] J. J. Wu, R. Molina, E. Oset and B. S. Zou, Prediction of narrow  $N^*$  and  $\Lambda^*$  resonances with hidden charm above 4 GeV, *Phys. Rev. Lett.* **105**, 232001 (2010).
- [17] W. L. Wang, F. Huang, Z. Y. Zhang, and B. S. Zou,  $\Sigma_c \bar{D}$  and  $\Lambda_c \bar{D}$  states in a chiral quark model, *Phys. Rev. C* **84**, 015203 (2011).
- [18] Z. C. Yang, Z. F. Sun, J. He, X. Liu, and S. L. Zhu, The possible hidden-charm molecular baryons composed of anti-charmed meson and charmed baryon, *Chin. Phys. C* **36**, 6 (2012).
- [19] J. J. Wu, T.-S. H. Lee, and B. S. Zou, Nucleon resonances with hidden charm in coupled-channel Models, *Phys. Rev. C* **85**, 044002 (2012).
- [20] X. Q. Li and X. Liu, A possible global group structure for exotic states, *Eur. Phys. J. C* **74**, 3198 (2014).
- [21] R. Chen, X. Liu, X. Q. Li, and S. L. Zhu, Identifying Exotic Hidden-Charmed Pentaquarks, *Phys. Rev. Lett.* **115**, 132002 (2015).
- [22] M. Karliner and J. L. Rosner, New Exotic Meson and Baryon Resonances from Doubly-Heavy Hadronic Molecules, *Phys. Rev. Lett.* **115**, 122001 (2015).
- [23] R. Aaij *et al.* (LHCb Collaboration), Evidence of a  $J/\psi \Lambda$  structure and observation of excited  $\Xi^-$  states in the  $\Xi_b^- \rightarrow J/\psi \Lambda K^-$  decay, *Sci. Bull.* **66**, 1278-1287 (2021).
- [24] R. Aaij *et al.* (LHCb Collaboration), Observation of a  $J/\psi \Lambda$  resonance consistent with a strange pentaquark candidate in  $B^- \rightarrow J/\psi \Lambda \bar{p}$  decays, *Phys. Rev. Lett.* **131**, 031901 (2023).
- [25] J. Hofmann and M. F. M. Lutz, Coupled-channel study of crypto-exotic baryons with charm, *Nucl. Phys. A* **763**, 90 (2005).
- [26] J. J. Wu, R. Molina, E. Oset and B. S. Zou, Dynamically generated  $N^*$  and  $\Lambda^*$  resonances in the hidden charm sector around 4.3 GeV, *Phys. Rev. C* **84**, 015202 (2011).
- [27] V. V. Anisovich, M. A. Matveev, J. Nyiri, A. V. Sarantsev, and A. N. Semenova, Nonstrange and strange pentaquarks with hidden charm, *Int. J. Mod. Phys. A* **30**, 1550190 (2015).
- [28] A. Feijoo, V. K. Magas, A. Ramos, and E. Oset, A hidden-charm  $S = -1$  pentaquark from the decay of  $\Lambda_b$  into  $J/\psi \eta \Lambda$  states, *Eur. Phys. J. C* **76**, no. 8, 446 (2016).
- [29] J. X. Lu, E. Wang, J. J. Xie, L. S. Geng, and E. Oset, The  $\Lambda_b \rightarrow J/\psi K^0 \Lambda$  reaction and a hidden-charm pentaquark state with strangeness, *Phys. Rev. D* **93**, 094009 (2016).
- [30] H. X. Chen, L. S. Geng, W. H. Liang, E. Oset, E. Wang, and J. J. Xie, Looking for a hidden-charm pentaquark state with strangeness  $S = -1$  from  $\Xi_b^-$  decay into  $J/\psi K^- \Lambda$ , *Phys. Rev. C* **93**, 065203 (2016).
- [31] R. Chen, J. He, and X. Liu, Possible strange hidden-charm pentaquarks from  $\Sigma_c^{(*)} \bar{D}_s^*$  and  $\Xi_c^{(*)} \bar{D}^*$  interactions, *Chin. Phys. C* **41**, 103105 (2017).
- [32] X. Z. Weng, X. L. Chen, W. Z. Deng and S. L. Zhu, Hidden-charm pentaquarks and  $P_c$  states, *Phys. Rev. D* **100**, no.1, 016014 (2019).
- [33] C. W. Xiao, J. Nieves, and E. Oset, Prediction of hidden charm strange molecular baryon states with heavy quark spin symmetry, *Phys. Lett. B* **799**, 135051 (2019).
- [34] B. Wang, L. Meng, and S. L. Zhu, Spectrum of the strange hidden charm molecular pentaquarks in chiral effective field theory, *Phys. Rev. D* **101**, 034018 (2020).
- [35] M. Karliner and J. L. Rosner, New strange pentaquarks, *Phys. Rev. D* **106**, no.3, 036024 (2022).
- [36] F. L. Wang and X. Liu, Emergence of molecular-type characteristic spectrum of hidden-charm pentaquark with strangeness embodied in the  $P_{\psi s}^\Lambda(4338)$  and  $P_{cs}(4459)$ , *Phys. Lett. B* **835**, 137583 (2022).
- [37] R. Aaij *et al.* (LHCb Collaboration), Observation of an exotic narrow doubly charmed tetraquark, *Nature Phys.* **18**, no.7, 751-754 (2022).
- [38] A. V. Manohar and M. B. Wise, Exotic  $QQ\bar{q}\bar{q}$  states in QCD, *Nucl. Phys. B* **399**, 17-33 (1993).
- [39] T. E. O. Ericson and G. Karl, Strength of pion exchange in hadronic molecules, *Phys. Lett. B* **309**, 426-430 (1993).
- [40] N. A. Tornqvist, From the deuteron to deusons, an analysis of deuteron-like meson-meson bound states, *Z. Phys. C* **61**, 525 (1994).
- [41] D. Janc and M. Rosina, The  $T_{cc} = DD^*$  molecular state, *Few Body Syst.* **35**, 175-196 (2004).
- [42] G. J. Ding, J. F. Liu and M. L. Yan, Dynamics of Hadronic Molecule in One-Boson Exchange Approach and Possible Heavy Flavor Molecules, *Phys. Rev. D* **79**, 054005 (2009).
- [43] R. Molina, T. Branz and E. Oset, A new interpretation for the  $D_{s2}^*(2573)$  and the prediction of novel exotic charmed mesons,

- Phys. Rev. D **82**, 014010 (2010).
- [44] S. Ohkoda, Y. Yamaguchi, S. Yasui, K. Sudoh and A. Hosaka, Exotic mesons with double charm and bottom flavor, *Phys. Rev. D* **86**, 034019 (2012).
- [45] N. Li, Z. F. Sun, X. Liu and S. L. Zhu, Coupled-channel analysis of The possible  $D^{(*)}D^{(*)}$ ,  $\bar{B}^{(*)}\bar{B}^{(*)}$  and  $D^{(*)}\bar{B}^{(*)}$  molecular states, *Phys. Rev. D* **88**, 114008 (2013).
- [46] H. Xu, B. Wang, Z. W. Liu and X. Liu,  $DD^*$  potentials in chiral perturbation theory and possible molecular states, *Phys. Rev. D* **99**, 014027 (2019).
- [47] M. Z. Liu, T. W. Wu, M. Pavon Valderrama, J. J. Xie and L. S. Geng, Heavy-quark spin and flavor symmetry partners of the  $X(3872)$  revisited: What can we learn from the one-boson exchange model?, *Phys. Rev. D* **99**, 094018 (2019).
- [48] L. Tang, B. D. Wan, K. Maltman and C. F. Qiao, Doubly Heavy Tetraquarks in QCD Sum Rules, *Phys. Rev. D* **101**, no.9, 094032 (2020).
- [49] Z. M. Ding, H. Y. Jiang and J. He, Molecular states from  $D^{(*)}\bar{D}^{(*)}/B^{(*)}\bar{B}^{(*)}$  and  $D^{(*)}D^{(*)}/\bar{B}^{(*)}\bar{B}^{(*)}$  interactions, *Eur. Phys. J. C* **80**, 1179 (2020).
- [50] R. Chen, N. Li, Z. F. Sun, X. Liu and S. L. Zhu, Doubly charmed molecular pentaquarks, *Phys. Lett. B* **822**, 136693 (2021).
- [51] N. Yalikun, X. K. Dong and B. S. Zou, Molecular states in  $D_s^{(*)+}\Xi_c^{('*,*)}$  systems, [arXiv:2303.03629](https://arxiv.org/abs/2303.03629).
- [52] F. L. Wang and X. Liu, New type of doubly charmed molecular pentaquarks containing most strange quarks: Mass spectra, radiative decays, and magnetic moments, *Phys. Rev. D* **108**, no.7, 074022 (2023).
- [53] R. Machleidt, K. Holinde and C. Elster, The Bonn Meson Exchange Model for the Nucleon Nucleon Interaction, *Phys. Rept.* **149**, 1-89 (1987).
- [54] E. Epelbaum, H. W. Hammer and U. G. Meissner, Modern Theory of Nuclear Forces, *Rev. Mod. Phys.* **81**, 1773-1825 (2009).
- [55] A. Esposito, A. L. Guerrieri, F. Piccinini, A. Pilloni and A. D. Polosa, Four-Quark Hadrons: an Updated Review, *Int. J. Mod. Phys. A* **30**, 1530002 (2015).
- [56] N. A. Tornqvist, On deusons or deuteron-like meson-meson bound states, *Nuovo Cim. Soc. Ital. Fis.* **107A**, 2471 (1994).
- [57] R. Chen, A. Hosaka and X. Liu, Prediction of triple-charm molecular pentaquarks, *Phys. Rev. D* **96**, no. 11, 114030 (2017).
- [58] F. L. Wang, R. Chen, Z. W. Liu, and X. Liu, Probing new types of  $P_c$  states inspired by the interaction between  $S$ -wave charmed baryon and anti-charmed meson in a  $\bar{T}$  doublet, *Phys. Rev. C* **101**, 025201 (2020).
- [59] F. Schlumpf, Magnetic moments of the baryon decuplet in a relativistic quark model, *Phys. Rev. D* **48**, 4478-4480 (1993).
- [60] F. Schlumpf, Relativistic constituent quark model of electroweak properties of baryons, *Phys. Rev. D* **47**, 4114 (1993); [*Phys. Rev. D* **49**, 6246 (1994)].
- [61] T. P. Cheng and L. F. Li, Why naive quark model can yield a good account of the baryon magnetic moments, *Phys. Rev. Lett.* **80**, 2789-2792 (1998).
- [62] P. Ha and L. Durand, Baryon magnetic moments in a QCD based quark model with loop corrections, *Phys. Rev. D* **58**, 093008 (1998).
- [63] Y. R. Liu, P. Z. Huang, W. Z. Deng, X. L. Chen and S. L. Zhu, Pentaquark magnetic moments in different models, *Phys. Rev. C* **69**, 035205 (2004).
- [64] P. Z. Huang, Y. R. Liu, W. Z. Deng, X. L. Chen and S. L. Zhu, Heavy pentaquarks, *Phys. Rev. D* **70**, 034003 (2004).
- [65] S. L. Zhu, Pentaquarks, *Int. J. Mod. Phys. A* **19**, 3439-3469 (2004).
- [66] S. Kumar, R. Dhir and R. C. Verma, Magnetic moments of charm baryons using effective mass and screened charge of quarks, *J. Phys. G* **31**, 141-147 (2005).
- [67] A. R. Haghpayma, Magnetic Moment of the Pentaquark  $\Theta^+$  State, [arXiv:hep-ph/0609253](https://arxiv.org/abs/hep-ph/0609253).
- [68] G. Ramalho, K. Tsushima and F. Gross, A Relativistic quark model for the Omega-electromagnetic form factors, *Phys. Rev. D* **80**, 033004 (2009).
- [69] R. Dhir and R. C. Verma, Magnetic Moments of ( $J^P = 3/2^+$ ) Heavy Baryons Using Effective Mass Scheme, *Eur. Phys. J. A* **42**, 243-249 (2009).
- [70] A. Majethiya, B. Patel and P. C. Vinodkumar, Radiative decays of single heavy flavour baryons, *Eur. Phys. J. A* **42**, 213-218 (2009).
- [71] N. Sharma, H. Dahiya, P. K. Chatley and M. Gupta, Spin  $\frac{1}{2}^+$ , spin  $\frac{3}{2}^+$  and transition magnetic moments of low lying and charmed baryons, *Phys. Rev. D* **81**, 073001 (2010).
- [72] N. Sharma, A. Martinez Torres, K. P. Khemchandani and H. Dahiya, Magnetic moments of the low-lying  $1/2^-$  octet baryon resonances, *Eur. Phys. J. A* **49**, 11 (2013).
- [73] R. Dhir, C. S. Kim and R. C. Verma, Magnetic Moments of Bottom Baryons: Effective mass and Screened Charge, *Phys. Rev. D* **88**, 094002 (2013).
- [74] Z. Ghalenovi, A. A. Rajabi, S. x. Qin and D. H. Rischke, Ground-State Masses and Magnetic Moments of Heavy Baryons, *Mod. Phys. Lett. A* **29**, 1450106 (2014).
- [75] A. Girdhar, H. Dahiya and M. Randhawa, Magnetic moments of  $J^P = \frac{3}{2}^+$  decuplet baryons using effective quark masses in chiral constituent quark model, *Phys. Rev. D* **92**, 033012 (2015).
- [76] A. Majethiya, K. Thakkar and P. C. Vinodkumar, Spectroscopy and decay properties of  $\Sigma_b, \Lambda_b$  baryons in quark-diquark model, *Chin. J. Phys.* **54**, 495-502 (2016).
- [77] K. Thakkar, A. Majethiya and P. C. Vinodkumar, Magnetic moments of baryons containing all heavy quarks in the quark-diquark model, *Eur. Phys. J. Plus* **131**, 339 (2016).
- [78] Z. Shah, K. Thakkar, A. K. Rai and P. C. Vinodkumar, Mass spectra and Regge trajectories of  $\Lambda_c^+, \Sigma_c^0, \Xi_c^0$  and  $\Omega_c^0$  baryons, *Chin. Phys. C* **40**, 123102 (2016).
- [79] Z. Shah, K. Thakkar and A. K. Rai, Excited State Mass spectra of doubly heavy baryons  $\Omega_{cc}, \Omega_{bb}$  and  $\Omega_{bc}$ , *Eur. Phys. J. C* **76**, 530 (2016).
- [80] G. J. Wang, R. Chen, L. Ma, X. Liu and S. L. Zhu, Magnetic moments of the hidden-charm pentaquark states, *Phys. Rev. D* **94**, no.9, 094018 (2016).
- [81] A. Kaur, P. Gupta and A. Upadhyay, Properties of  $J^P = 1/2^+$  baryon octets at low energy, *PTEP* **2017**, 063B02 (2017).
- [82] Z. Shah and A. Kumar Rai, Spectroscopy of the  $\Omega_{ccb}$  baryon in the hypercentral constituent quark model, *Chin. Phys. C* **42**, 053101 (2018).
- [83] K. Gandhi, Z. Shah and A. K. Rai, Decay properties of singly charmed baryons, *Eur. Phys. J. Plus* **133**, 512 (2018).
- [84] H. Dahiya, Transition magnetic moments of  $J^P = \frac{3}{2}^+$  decuplet to  $J^P = \frac{1}{2}^+$  octet baryons in the chiral constituent quark model, *Chin. Phys. C* **42**, 093102 (2018).
- [85] V. Simonis, Improved predictions for magnetic moments and M1 decay widths of heavy hadrons, [arXiv:1803.01809](https://arxiv.org/abs/1803.01809).
- [86] Z. Ghalenovi and M. Moazzen Sorkhi, Mass spectra and decay properties of  $\Sigma_b$  and  $\Lambda_b$  baryons in a quark model, *Eur. Phys. J. Plus* **133**, 301 (2018).
- [87] K. Gandhi and A. K. Rai, Spectrum of strange singly charmed

- baryons in the constituent quark model, *Eur. Phys. J. Plus* **135**, 213 (2020).
- [88] S. Rahmani, H. Hassanabadi and H. Sobhani, Mass and decay properties of double heavy baryons with a phenomenological potential model, *Eur. Phys. J. C* **80**, 312 (2020).
- [89] A. Hazra, S. Rakshit and R. Dhir, Radiative M1 transitions of heavy baryons: Effective quark mass scheme, *Phys. Rev. D* **104**, 053002 (2021).
- [90] C. Menapara and A. K. Rai, Spectroscopic investigation of light strange  $S = -1$   $\Lambda$ ,  $\Sigma$  and  $S = -2$   $\Xi$  baryons, *Chin. Phys. C* **45**, 063108 (2021).
- [91] M. W. Li, Z. W. Liu, Z. F. Sun and R. Chen, Magnetic moments and transition magnetic moments of  $P_c$  and  $P_{cs}$  states, *Phys. Rev. D* **104**, no.5, 054016 (2021).
- [92] H. Y. Zhou, F. L. Wang, Z. W. Liu and X. Liu, Probing the electromagnetic properties of the  $\Xi_c^{(*)} D^{(*)}$ -type doubly charmed molecular pentaquarks, *Phys. Rev. D* **106**, no.3, 034034 (2022).
- [93] F. L. Wang, H. Y. Zhou, Z. W. Liu and X. Liu, What can we learn from the electromagnetic properties of hidden-charm molecular pentaquarks with single strangeness?, *Phys. Rev. D* **106**, 054020 (2022).
- [94] F. L. Wang, S. Q. Luo, H. Y. Zhou, Z. W. Liu and X. Liu, Exploring the electromagnetic properties of the  $\Xi_c^{(*)} \bar{D}_s^*$  and  $\Omega_c^{(*)} \bar{D}_s^*$  molecular states, *Phys. Rev. D* **108**, 034006 (2023).
- [95] C. Deng and S. L. Zhu,  $T_{cc}^+$  and its partners, *Phys. Rev. D* **105**, no.5, 054015 (2022).
- [96] F. Gao and H. S. Li, Magnetic moments of the hidden-charm strange pentaquark states, *Chin. Phys. C* **46**, no.12, 123111 (2022).
- [97] C. Menapara and A. K. Rai, Spectroscopic Study of Strangeness =  $-3$   $\Omega^-$  Baryon, *Chin. Phys. C* **46**, 103102 (2022).
- [98] H. Mutuk, The status of  $\Xi_{cc}^{++}$  baryon: investigating quark-diquark model, *Eur. Phys. J. Plus* **137**, 10 (2022).
- [99] A. Kakadiya, Z. Shah and A. K. Rai, Spectroscopy of  $\Omega_{ccc}$  and  $\Omega_{bbb}$  baryons, *Int. J. Mod. Phys. A* **37**, no.36, 2250225 (2022).
- [100] C. Menapara and A. K. Rai, Spectroscopy of light baryons:  $\Delta$  resonances, *Int. J. Mod. Phys. A* **37**, no.27, 2250177 (2022).
- [101] B. Mohan, T. M. S., A. Hazra and R. Dhir, Screening of the quark charge and mixing effects on transition moments and M1 decay widths of baryons, *Phys. Rev. D* **106**, no.11, 113007 (2022).
- [102] H. T. An, S. Q. Luo, Z. W. Liu and X. Liu, Spectroscopy behavior of fully heavy tetraquarks, *Eur. Phys. J. C* **83**, 740 (2023).
- [103] T. W. Wu and Y. L. Ma, Doubly heavy tetraquark multiplets as heavy antiquark-diquark symmetry partners of heavy baryons, *Phys. Rev. D* **107**, no.7, L071501 (2023).
- [104] F. L. Wang, S. Q. Luo and X. Liu, Radiative decays and magnetic moments of the predicted  $B_c$ -like molecules, *Phys. Rev. D* **107**, no.11, 114017 (2023).
- [105] M. B. Wise, Chiral perturbation theory for hadrons containing a heavy quark, *Phys. Rev. D* **45**, R2188 (1992).
- [106] R. Casalbuoni, A. Deandrea, N. Di Bartolomeo, R. Gatto, F. Feruglio, and G. Nardulli, Light vector resonances in the effective chiral Lagrangian for heavy mesons, *Phys. Lett. B* **292**, 371 (1992).
- [107] T. M. Yan, H. Y. Cheng, C. Y. Cheung, G. L. Lin, Y. C. Lin, and H. L. Yu, Heavy quark symmetry and chiral dynamics, *Phys. Rev. D* **46**, 1148 (1992); [*Phys. Rev. D* **55**, 5851E (1997)].
- [108] R. Casalbuoni, A. Deandrea, N. Di Bartolomeo, R. Gatto, F. Feruglio, and G. Nardulli, Phenomenology of heavy meson chiral Lagrangians, *Phys. Rep.* **281**, 145 (1997).
- [109] M. Bando, T. Kugo and K. Yamawaki, Nonlinear Realization and Hidden Local Symmetries, *Phys. Rept.* **164**, 217 (1988).
- [110] M. Harada and K. Yamawaki, Hidden local symmetry at loop: A New perspective of composite gauge boson and chiral phase transition, *Phys. Rept.* **381**, 1 (2003).
- [111] R. Chen, A. Hosaka, and X. Liu, Searching for possible  $\Omega_c$ -like molecular states from meson-baryon interaction, *Phys. Rev. D* **97**, 036016 (2018).
- [112] G. J. Ding, Are  $Y(4260)$  and  $Z_2^+(4250)$   $D_1 D$  or  $D_0 D^*$  hadronic molecules? *Phys. Rev. D* **79**, 014001 (2009).
- [113] D. O. Riska and G. E. Brown, Nucleon resonance transition couplings to vector mesons, *Nucl. Phys. A* **679**, 577 (2001).
- [114] R. Chen, F. L. Wang, A. Hosaka and X. Liu, Exotic triple-charm deuteronlike hexaquarks, *Phys. Rev. D* **97**, 114011 (2018).
- [115] R. Chen, Z. F. Sun, X. Liu and S. L. Zhu, Strong LHCb evidence supporting the existence of the hidden-charm molecular pentaquarks, *Phys. Rev. D* **100**, no. 1, 011502 (2019).
- [116] F. L. Wang and X. Liu, Exotic double-charm molecular states with hidden or open strangeness and around  $4.5 \sim 4.7$  GeV, *Phys. Rev. D* **102**, 094006 (2020).
- [117] F. L. Wang and X. Liu, Investigating new type of doubly charmed molecular tetraquarks composed of charmed mesons in the  $H$  and  $T$  doublets, *Phys. Rev. D* **104**, no.9, 094030 (2021).
- [118] F. L. Wang, X. D. Yang, R. Chen and X. Liu, Correlation of the hidden-charm molecular tetraquarks and the charmoniumlike structures existing in the  $B \rightarrow XYZ + K$  process, *Phys. Rev. D* **104**, no.9, 094010 (2021).
- [119] F. L. Wang, R. Chen, and X. Liu, Prediction of hidden-charm pentaquarks with double strangeness, *Phys. Rev. D* **103**, 034014 (2021).
- [120] F. L. Wang, X. D. Yang, R. Chen and X. Liu, Hidden-charm pentaquarks with triple strangeness due to the  $\Omega_c^{(*)} \bar{D}_s^{(*)}$  interactions, *Phys. Rev. D* **103**, 054025 (2021).
- [121] X. D. Yang, F. L. Wang, Z. W. Liu and X. Liu, Newly observed  $X(4630)$ : a new charmoniumlike molecule, *Eur. Phys. J. C* **81**, no.9, 807 (2021).
- [122] R. Chen, Can the newly reported  $P_{cs}(4459)$  be a strange hidden-charm  $\Xi_c \bar{D}^*$  molecular pentaquark?, *Phys. Rev. D* **103**, no.5, 054007 (2021).
- [123] F. L. Wang, R. Chen and X. Liu, A new group of doubly charmed molecule with  $T$ -doublet charmed meson pair, *Phys. Lett. B* **835**, 137502 (2022).
- [124] F. L. Wang and X. Liu, Higher molecular  $P_{\psi_s}^{\Lambda/\Sigma}$  pentaquarks arising from the  $\Xi_c^{(*)} \bar{D}_1 / \Xi_c^{(*)} \bar{D}_2^*$  interactions, *Phys. Rev. D* **108**, no.5, 054028 (2023).
- [125] R. L. Workman *et al.* [Particle Data Group], Review of Particle Physics, *PTEP* **2022**, 083C01 (2022).
- [126] V. B. Berestetsky, E. M. Lifshitz, and L. P. Pitaevsky, Quantum Electrodynamics, Pergamon Press, 1982, ISBN 978-0-7506-3371-0.
- [127] F. L. Wang, R. Chen, Z. W. Liu, and X. Liu, Possible triple-charm molecular pentaquarks from  $\Xi_{cc} D_1 / \Xi_{cc} D_2^*$  interactions, *Phys. Rev. D* **99**, 054021 (2019).
- [128] X. K. Dong, F. K. Guo and B. S. Zou, A survey of heavy-heavy hadronic molecules, *Commun. Theor. Phys.* **73**, no.12, 125201 (2021).
- [129] G. L. Yu, Z. Y. Li, Z. G. Wang, J. Lu and M. Yan, Systematic analysis of doubly charmed baryons  $\Xi_{cc}$  and  $\Omega_{cc}$ , *Eur. Phys. J. A* **59**, no.6, 126 (2023).

- [130] J. Dey, V. Shevchenko, P. Volkovitsky and M. Dey, Radiative decays of  $S$ -wave charmed baryons, *Phys. Lett. B* **337**, 185-188 (1994).
- [131] S. Q. Luo and X. Liu, Investigating the spectroscopy behavior of undetected  $1F$ -wave charmed baryons, *Phys. Rev. D* **108**, no.3, 034002 (2023).
- [132] V. K. Khersonskii, A. N. Moskalev and D. A. Varshalovich, Quantum Theory Of Angular Momentum, *World Scientific Publishing Company, Singapore*, 1988.
- [133] T. M. Aliev, K. Azizi and A. Ozpineci, Radiative Decays of the Heavy Flavored Baryons in Light Cone QCD Sum Rules, *Phys. Rev. D* **79**, 056005 (2009).
- [134] V. Šimonis, Magnetic properties of ground-state mesons, *Eur. Phys. J. A* **52**, no.4, 90 (2016).
- [135] L. Y. Glozman and D. O. Riska, The Charm and bottom hyperons and chiral dynamics, *Nucl. Phys. A* **603**, 326-344 (1996);  
[erratum: *Nucl. Phys. A* **620**, 510-510 (1997)].
- [136] W. X. Zhang, H. Xu and D. Jia, Masses and magnetic moments of hadrons with one and two open heavy quarks: Heavy baryons and tetraquarks, *Phys. Rev. D* **104**, no.11, 114011 (2021).
- [137] B. Patel, A. K. Rai and P. C. Vinodkumar, Masses and magnetic moments of heavy flavour baryons in hyper central model, *J. Phys. G* **35**, 065001 (2008).
- [138] N. Barik and M. Das, Magnetic moments of confined quarks and baryons in an independent quark model based on Dirac equation with power law potential, *Phys. Rev. D* **28**, 2823-2829 (1983).
- [139] R. Aaij *et al.* (LHCb Collaboration), Physics case for an LHCb Upgrade II-Opportunities in flavour physics, and beyond, in the HL-LHC era, [arXiv:1808.08865](https://arxiv.org/abs/1808.08865).